Coupled geophysical and technoeconomic growth constraints on geological carbon storage scaleup with an application to the UK

Iman R. Kivi[1,2*], Xiaowei Gao[2], Samuel Krevor[2]

[1]Global Change Research Group (GCRG), IMEDEA-CSIC-UIB, Esporles, Spain

[2]Department of Earth Science and Engineering, Imperial College London, London, UK

*Email of the corresponding author: iman.rahimzadeh@uib.es

Abstract

Geological carbon dioxide storage is central to meeting many national climate change commitments. Yet large-scale deployment remains poorly constrained by both techno-economic limits on how rapidly the technology can scale and physics-based constraints imposed by the behavior of the subsurface. We here develop a modelling framework to identify feasible CO_2 storage scaleup trajectories constrained simultaneously by techno-economic growth and dynamic geophysical limits. We employ logistic and Gompertz models to represent policy-compliant deployment trajectories and simplified physics models to assess the resulting regional subsurface pressurisation. Applying the framework to the United Kingdom (UK), we find that offshore storage resources are sufficient to accommodate all government mid-century deployment rate targets up to 175 Mt yr^{-1}. Cumulative storage of up to 78 Gt can be achieved under Gompertz growth trajectories. The more aggressive logistic trajectories are constrained by reservoir injectivity, limiting the achievable resource base to 69 Gt. Geological uncertainties further narrow feasible pathways, but does not eliminate many key scaleup targets. A tenfold reduction in reservoir permeability while maintaining mid-century injection rates decreases the achievable storage resource to ~40 Gt. We conclude that a large contribution from geological

CO_2 storage to rapid decarbonisation in the UK is attainable if supporting regulation, investment and industrial capacity expand in accordance with national climate ambitions.

Keywords: Climate change mitigation; Growth modelling; Geophysical constraints; Simplified-physics modelling; United Kingdom decarbonization roadmap; Storage resource

1. Introduction

The majority of climate change mitigation pathways require large-scale deployment of carbon dioxide storage in deep geological formations.[1-5] The United Kingdom (UK) similarly incorporates geological CO_2 storage as a central component of its decarbonisation strategy, targeting storage rates of 20-30 Megatonnes (Mt) CO_2 y^{-1} by 2030 and 75-175 Mt CO_2 yr^{-1} by 2050.[6] The UK is uniquely positioned to plan such large-scale storage given its abundant offshore resources in the North Sea, which offer the potential to serve as a regional CO_2 storage hub for Europe.[7] The envisioned storage rates are comparable to the fluid-handling scales of the hydrocarbon industry–nearly 57 Mt of oil equivalent were produced from the UK sector of the North Sea in 2023[8]– underscoring the extent of the industrial transformation required to meet UK national climate targets.

Integrated assessment models are the primary tools used to project CO_2 storage deployment within climate mitigation pathways.[2] These models combine knowledge from different domains to assess how CO_2 storage influences the climate and economy.[9,10] They typically determine the CO_2 storage contribution to emission abatement through technoeconomic optimisation of energy systems, with relative technology costs acting as the main constraint.[11] Some modelling frameworks may impose global upper bounds on available storage capacity or annual injection rates, thereby incorporating a simplified representation of geophysical limits.[12-15] Storage resource estimates used in integrated assessment models are

commonly based on volumetric evaluations of rock pore space, combined with a storage efficiency factor to address CO_2 flow and trapping dynamics underground.[16] Such approaches sometimes fail to capture dynamic physical processes that may limit use of the resource, including reservoir pressurisation, CO_2 flow, and the geomechanical response of the storage complex.[17] Accounting for these factors may substantially impact estimates of both ultimate storage capacities and sustainable injection rates, since excess reservoir pressure buildup may threaten storage complex integrity or induce earthquakes,[18,19] and migrating CO_2 plumes may elevate leakage risk if they intersect legacy wells and permeable faults.[20,21]

Beyond geophysical uncertainties in storage resource use, another critical factor overlooked by integrated assessment models is a realistic representation of the sustained development rates at which CO_2 storage deployment can occur.[15,22-26] Globally, CO_2 storage deployment is experiencing rapid growth, resembling the early-stage expansion of large-scale energy infrastructure such as the petroleum industry in the early- to mid-20th century.[27-29] Yet, historical industrial analogues show that such rapid growth is rarely sustained over the decades in the way projected by some integrated assessment models.[30,31] Indeed, integrated assessment models underrepresent key techno-socio-economic constraints on CO_2 storage scaleup, including project development timelines, siting, property rights, regulatory approvals, financing and public acceptance.[32,33] Thus, the feasibility of delivering geological CO_2 storage at scales implied by climate targets remains highly uncertain, hinging on the interplay between achievable growth rates and the physical limits to safe injection.

To study CO_2 storage scaleup challenges a number of scalable modelling frameworks have been developed. For the representation of techno-economic limitations, logistic growth models, originally developed to describe the expansion of extractive resource technologies,[34,35] provide a useful means to capture the dynamics of CO_2 storage.[15,22,23,26] For the representation of geophysical processes, simplified-physics models have been developed to capture reservoir

pressurisation and CO_2 plume migration underground over regional scales.[17,18,36,37] Combining these two modelling frameworks enables an analysis of the temporal limits on the scaleup of geological CO_2 storage. Fuhrman et al. (2025)[22] show that when implementing combined growth and maximum total injectivity constraints into an integrated assessment modeling framework, the CO_2 storage deployment is globally reduced. Combining technological growth constraints from the rate of injection well construction with pressure constraints on geological CO_2 storage scaleup for the UK, de Jonge-Anderson et al. (2026)[38] find that the rate of well construction is the limiting constraint on scaleup relative to projected mitigation pathways.

In this paper, we advance the identification of feasible scaleup trajectories for CO_2 storage by combining models of technological and geophysical constraints into a single framework. In our framework, growth models (symmetric and asymmetric logistic curves) represent the techno-economic limits to CO_2 storage deployment required to meet climate change mitigation roadmaps outlined for the UK. Simplified physics models of reservoir pressurization are used to identify those growth trajectories that can be achieved without unsafe pressurisation of the reservoir systems in which storage is taking place. Combined constraints in techno-economic growth and dynamic geophysics for CO_2 storage have been embedded into the modelling approaches of Fuhrman et al. (2025)[22], de Jonge-Anderson et al. (2026)[38], and Szulczewski et al., (2012)[17]. However, in this work we have developed a framework which both simplifies and generalizes this concept. Our modelling framework avoids the arbitrary selection of saturation points in the growth curves by using the assessed storage resource base, and it is more broadly applicable by enabling the adoption of patterns of growth observed in any or a range of industrial analogues, and is not constrained to a single empirical dataset, e.g., of well construction or historical oil and gas production, but rather a range of patterns can be used to quantify the impacts of uncertainty. We show how a single storage resource estimate arises naturally from the framework, identifying the resource base that can realistically be

achieved under plausible growth trajectories, over timescales of relevance to climate change mitigation roadmaps. Applying this framework to the United Kingdom, we find that scaleup is limited not by the size of the storage resource, but in achieving the rates of industrial expansion required to deliver these deployment pathways.

2. Methodology

2.1. Logistic growth modelling framework

To bridge the gap between near-term growth rates of geological carbon storage and long-term geophysical limits given finite subsurface storage resources, we employ phenomenological S-curve growth models to construct a feasibility envelope for CO_2 storage deployment in the UK. This approach is grounded in the historical evidence of analogous extractive and energy industries, where sigmoidal growth functions have proven robust in characterising production lifecycles constrained by finite resources.[27,34,39]

Adapting this framework to geological carbon storage, we build upon the methodology established by Zahasky and Krevor (2020)[26] and its application for the UK and global scaling studies.[7,15] Those studies relied on the symmetric logistic model, which has a rate of decline that mirrors the rate of growth. To capture the potential asymmetry in industrial scaleup, where the pace of infrastructure decommissioning or stabilisation may differ from that of initial expansion, we extend this framework by also using the Gompertz growth model, an instance of the generalised logistic model, for non-symmetric deployment trajectories. Drawing on analogue analyses of wind power and other energy technologies,[40,41] this dual-model approach enables the construction of a feasibility envelope that encompasses growth trajectories with historical precedent.

In the logistic formulation, the cumulative storage trajectory $P(t)$ and its corresponding injection rate $Q(t)$ are defined as

$$P(t) = \frac{C}{1+\exp\{r(t_p-t)\}}, \quad \text{Eq. (1)}$$

$$Q(t) = \frac{C \cdot r \cdot \exp(r(t_p-t))}{(1+\exp(r(t_p-t))^2}, \quad \text{Eq. (2)}$$

where C (Gt) is an asymptotic cumulative storage bound, r (yr^{-1}) is intrinsic growth constant that controls the curvature, i.e., the steepness, of the scaleup trajectory, t_p (yr) is the year at which $Q(t)$ reaches its maximum peak rate. The inflection point of the rate curve on the growth limb occurs at (Fig. 1)

$$t_n = t_p - ln(\frac{2+\sqrt{3}}{r}) \quad \text{Eq. (3)}$$

This parameter provides model-internal marker for the end of the strongly accelerating, near-exponential build-out phase.

To represent bounded but non-symmetric scaleup shapes, a Gompertz growth trajectory is defined as

$$P(t) = C\ \exp[-\exp\{r(t_p - t)\}], \quad \text{Eq. (4)}$$

$$Q(t) = C \cdot r \cdot \exp(r(t_p - t)) \cdot \exp[-\exp\{r(t_p - t)\}], \quad \text{Eq. (5)}$$

$$t_n = t_p - ln(\frac{3+\sqrt{5}}{2r}). \quad \text{Eq. (6)}$$

Both of these models are constrained by the same three parameters (C, r, and t_p in Eqs. 1,2). The key difference is that the symmetric curves have a higher peak in the storage rate at an earlier time (Fig. 1). For an equal storage resource base, the symmetric logistic curve will have trajectories that reach higher peak injection rates that are more likely to fall afoul of

geophysical limits as compared with the asymmetric Gompertz curves. From that perspective, the use of symmetric logistic curves results in conservative outcomes for the assessment of the feasibility of storage rate targets. In other words, if a storage rate target is identified as feasible along a symmetric logistic trajectory, it will also be feasible along the Gompertz trajectory with the same parameterisation – growth rate, 2050 target, and total resource base.

With both of the growth models, while r is the intrinsic shape parameter used to compute t_n and t_p, it is not necessarily equal to an empirically interpretable percentage growth per year for deployment. To describe the effective early-phase scaleup rate in a way that is comparable across models, we therefore define a compound annual growth rate, g, for cumulative storage over an explicitly defined early interval $[t_0, t_n]$ as

$$g_{P[t_0,t_n]} = \left(\frac{P_{(t_n)}}{P_{(t_0)}}\right)^{1/(t_n-t_0)} - 1 \qquad \text{Eq. (7)}$$

As such, g is used as a descriptive metric of pre-t_n build-out intensity, whereas r remains the model parameter that governs curvature and enables consistent calculation of timing metrics (including t_n).

These *S*-curve models represent growth resulting from the aggregate affect of specific policy instruments, market incentives, financing conditions, engineering activities, and regulatory processes, but in this work we do not identify these specific contributions. Instead, the logistic models provide simplified and smoothed (averaged) scaleup trajectories, with empirical basis in past industrial developments, and representative of the aggregate impact of these processes on the deployment.[7]

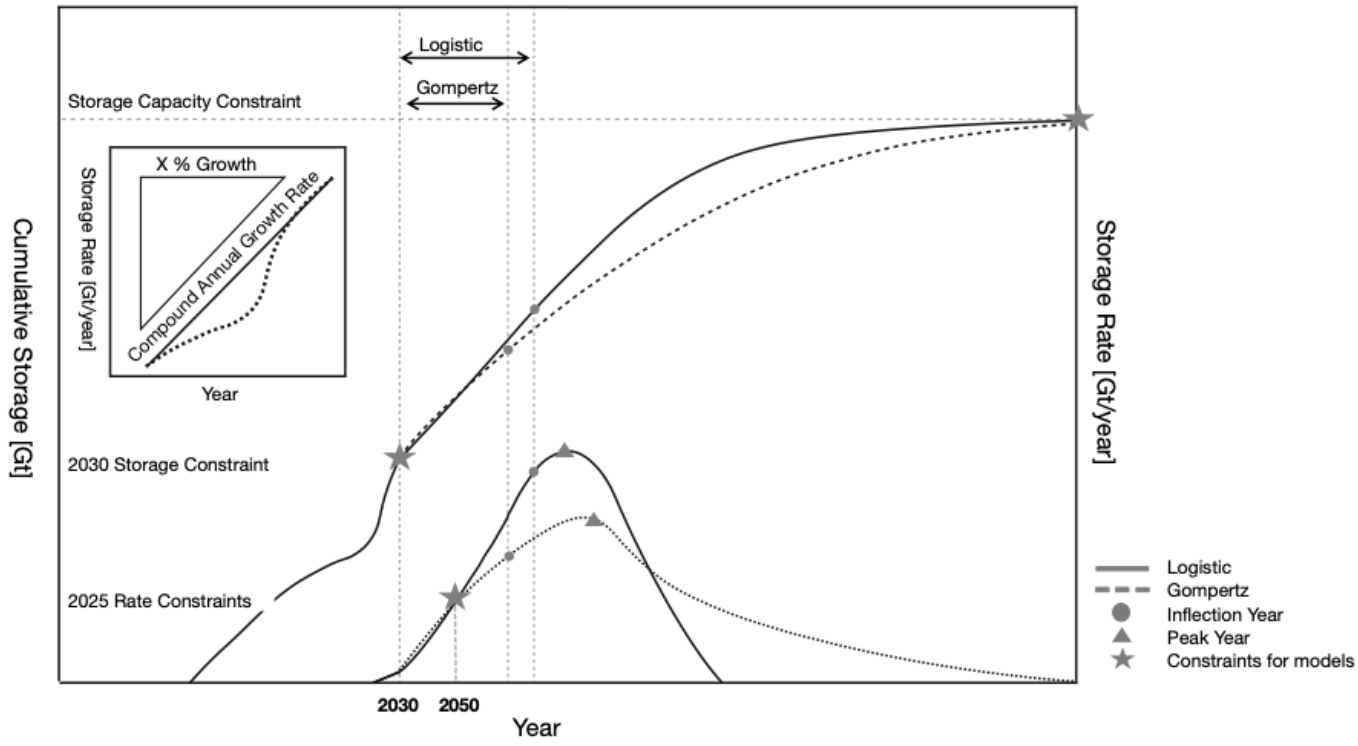

Fig. 1. Schematic illustration of the logistic and Gompertz growth models for geologic carbon storage and related model parameters. The figure highlights key parameters, and modelling constraints.

2.2. Parameters for the growth models

The models in Equations 1 and 2 are in their standard form with parameters C, r, and t_p. We parameterise C directly as described below, but parameterise the models with two other constraints that are of practical interest, and then solve for r and t_p. Firstly, we treat cumulative storage by 2030 as the take-off point for the UK scaleup pathways. Accordingly, we set $P(2030)$ equal to 0.385 Gt CO_2, derived from the UK project pipeline capacity.[42] To bound cumulative storage, we set the geological capacity to C = 78 Gt CO_2. This value is consistent with UK-wide storage assessments and is also used as a headline estimate in UK Government communications on offshore CO_2 storage potential.[43] Note that the parameter C represents a

static geophysical constraint, it is the maximum cumulative storage that can occur. However, the dynamic geophysical constraints arise from the distinct physics model, described in detail in §2.3. Finally, a policy-derived constraint is imposed on the storage rate in 2050. We consider three alternative mid-century targets Q_{2050} equal to 75, 130, and 175 Mt CO_2 y^{-1}, consistent with the range reported in the UK Climate Change Committee's Net Zero advice.[44] Each value is treated as a separate scenario, allowing the implied scaleup requirements to be compared under the same capacity ceiling and near-term take-off point.

For each Q_{2050} scenario, we numerically solve for r and t_p by requiring the model to satisfy both anchors simultaneously. We then impose a timing constraint used in recent feasibility-envelope studies by requiring the peak year to occur no earlier than mid-century, i.e, $t_p \geq 2050$.[7] This condition keeps the 2050 rate targets on the rising limb of the trajectory and avoids calibrations that would imply an early onset of decline within the period where the analysis is intended to represent sustained scaleup. One motivation for this constraint is to reflect the practical difficulty in the creation of a business environment that would enable the exploition of a natural resource close to the extent of the resource base. The resulting trajectories should thus be interpreted as accurate representations of multi-decadal averaged pathways, but do not reflect the short-term (1–5 year) fluctuations that occur within any industry.

2.3. Dynamic geophysical constraints

Subsurface pressure buildup represents the main dynamic geophysical constraint on regional CO_2 storage implementation and is thus the main focus of this modelling framework. Thus in the second stage of our modelling framework we assess whether the projected CO_2 storage scaleup trajectories in the UK derived from the logistic and Gompertz growth models (§2.2) are limited by basin-wide pressurisation. To carry out this analysis we have made developments

to the analytical tool CO2BLOCK[18,45] (see §S1 in Supporting Information for detailed explanation). We combine CO2BLOCK with the growth models to allocate the estimated storage resources under geophysical constraints to the projected CO_2 storage scaleup trajectories in the UK. This modelling framework is named CO2BLOCK-GROWTH and is publicly available as open source software with the link provided under the data availability statement.

This dynamic resource allocation problem is governed by (1) the characteristic shape of the symmetric and asymmetric growth trajectories, featuring an increase over time, reaching a peak, and subsequently declining, and (2) the effective storage capacity of each geological unit, which depends on the injection duration and the associated subsurface pressure dynamics. To comply with these constraints, we implement a sequential allocation procedure and obtain end member results by evaluating the use of storage units in either descending or ascending order of capacity, discussed in detail below. For example, in the descending approach, the geological unit with the largest estimated storage resource is assigned first and remains active throughout the entire modelled period.

The allocation logic involves finding in consecutive steps a constant injection rate such that the injected CO_2 mass matches that targeted by the growth trajectory (Fig. 2). This approach relies on the principle that if the required volume can be injected at a constant rate, it can also be addressed under variable but lower rates of scaleup trajectories over longer durations, as the maximum pressure buildup attenuates with time. The remaining part of the injection trajectory is then matched by successively assigning the next units until fully covering the area beneath the injection rate curve, representing the total projected CO_2 mass.

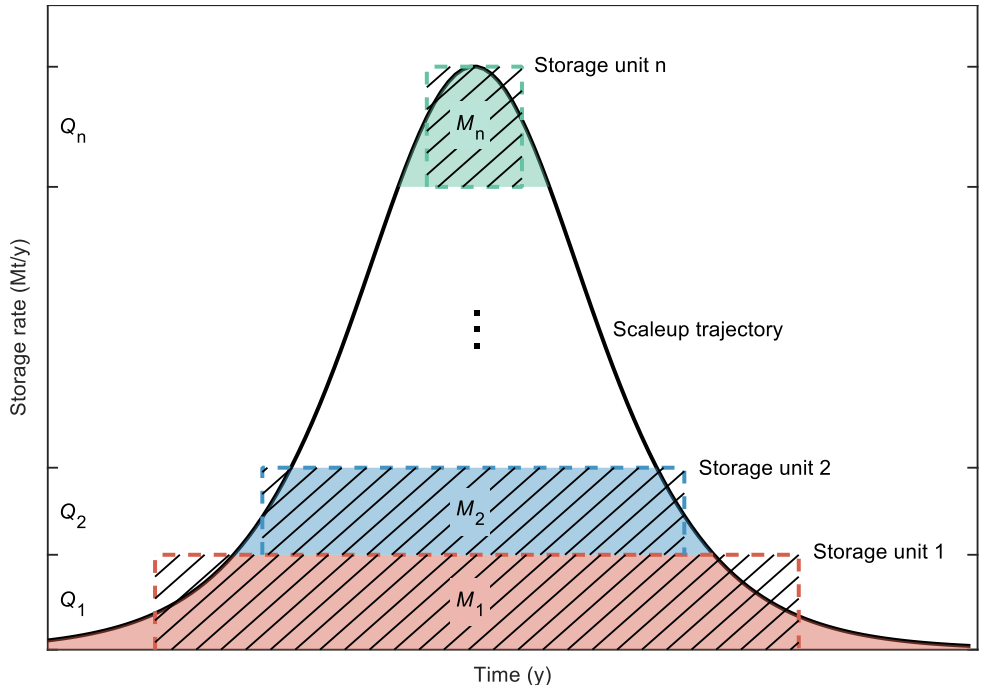

Fig. 2. Schematic illustration of the workflow for simulating the use of CO_2 storage resources along scaleup trajectories. The growth curve (in this case a symmetric logistic curve) serves as an envelope trajectory. Injection into individual geological units are then simulated at a constant maximum, across an optimum site number and spacing, where reservoir pressure does not exceed safe limits for rock failure and seismicity over the time period of consideration. Storage units are added such that the sum total CO_2 mass M (sum of the hatched surfaces) equals the value prescribed by the scaleup trajectory.

Real world development scenarios are unknown and will exhibit some convolution of spatial organization, e.g., due to locations of CO_2 transportation infrastructure and high quality storage resources, and random distribution reflecting the outcomes of market and policy driven processes like contract and license awards. To avoid arbitrary decision making in our modelling as mentioned earlier we apply two allocation strategies that are unrealistic in their spatial development of storage resources, but that represent end-member scenarios in terms of the geophysical limitations. Thus, these scenarios will encompass the range of plausible real world development scenarios in so far as inejctivity limitations are concerned.

The first adopted resource allocation strategy represents a geophysically favourable configuration, where locations are developed in order of decreasing capacity. The first storage units have the largest permeability, areal extent and thickness, minimising rates of pressure buildup. We also refer to this as the reference allocation strategy. The second end member scenario is one in which the resources are allocated in order of ascending capacity, i.e., the least favourable locations are developed first. We demonstrate that these are indeed end-member scenarios by also simulating random allocations of the storage resources.

Uncertainties also arise from the feasibility of developing a sufficient number of injection sites to fully utilise storage resources. The number of injection sites are primarily governed by the flow properties of the storage aquifers, which modulate pressure changes and may vary from one region to another. We also apply a minimum per site injection rate of 1 Mt yr^{-1} for economic viability of site development and a maximum of 20 Mt yr^{-1} acknowledging potential technological limitations.

To address site construction constraints, we draw an analogy with historical wellbore drilling for hydrocarbon production in the studied regions, providing a realistic benchmark for the number of wells that can be drilled within projected injection timeframes. We spatially correlate more than 13,000 hydrocarbon wellbores in the UK Continental Shelf[46] with candidate CO_2 storage units, considering both their geographic distribution and target geological formations. This correlation provides an estimate of the number of wellbores uniquely associated with each storage unit (see the distribution in Fig. S3). We translate this into a corresponding number of potential injection sites assuming that each injection site comprises, on average, three wellbores. We then adapt the reference resource allocation scenario by constraining the maximum number of injection sites in each region based on historically observed drilling activity.

Finally, we consider a resource allocation order informed by published plans for CO_2 storage projects in the UK. The first UK carbon storage licensing round in 2023 resulted in 21 licences awarded to 14 companies across the UK Continental Shelf, with additional licences from the second round expected in 2027 (see the distribution in Fig. 3).[47] Focusing on storage in saline aquifers, the awarded licences indicate that near-term deployment is likely to occur initially in the Southern North Sea, where the Endurance project targets the Bunter Sandstone aquifer.[48] This region also hosts licensed projects such as Viking CCS and Poseidon CCS, which primarily exploit depleted gas fields.[49] The East Irish Sea is expected to follow via the HyNet North West project, which initially targets depleted hydrocarbon reservoirs but envisions future expansion into saline aquifer storage. In the Central North Sea, the Acorn project is advancing appraisal of the Mey Sandstone and Captain Sandstone aquifers, providing additional large-scale saline storage potential.[50] The Northern North Sea, despite holding awarded licences for prospective aquifer storage, is expected to progress later due to its greater distance from shore, more limited cluster connectivity, and comparatively earlier appraisal stage of saline prospects. Accordingly, we consider resource allocation in the sequence: Southern North Sea, East Irish Sea, Central North Sea, and Northern North Sea.

2.4. Geologic storage units

Data of the storage units are mostly compiled from the CO_2Stored database.[51,52] This dataset provides information at higher spatial resolution than the comparable dataset published by the Geological Service for Europe.[53] The database contains the parameters required to model reservoir pressure buildup, including storage unit geometry, depth, porosity, permeability, and average reservoir pore pressure, temperature, and salinity. While the database provides estimates of the overburden stress, additional geomechanical parameters required to assess rock

failure thresholds, including horizontal in situ stress and rock failure properties, are compiled from published field measurements (explained in detail in §S2). Furthermore, to assess the sensitivity of storage resource estimates to uncertainty in reservoir permeability, we consider three scenarios in which permeability is reduced by factors of 2, 5, and 10 relative to the reference values from the database while keeping all other parameters unchanged (hereafter denoted $k/2$, $k/5$ and $k/10$, respectively).

We consider CO_2 storage in saline aquifers, which dominate total storage capacity in the UK. We constrain candidate storage units by considering those with (1) porosity higher than 10%, (2) permeability higher than 1 mD, (3) storage depth greater than 1000 m, where CO_2 is in supercritical phase to ensure storage efficiency, and (4) total theoretical storage capacity higher than 200 Mt. During this initial screening, the number of potential storage units reduces from 292 saline aquifers initially in the database to 27. All storage units are located offshore, with the majority in the UK sector of the North Sea and only one in the East Irish Sea (Fig. 3).

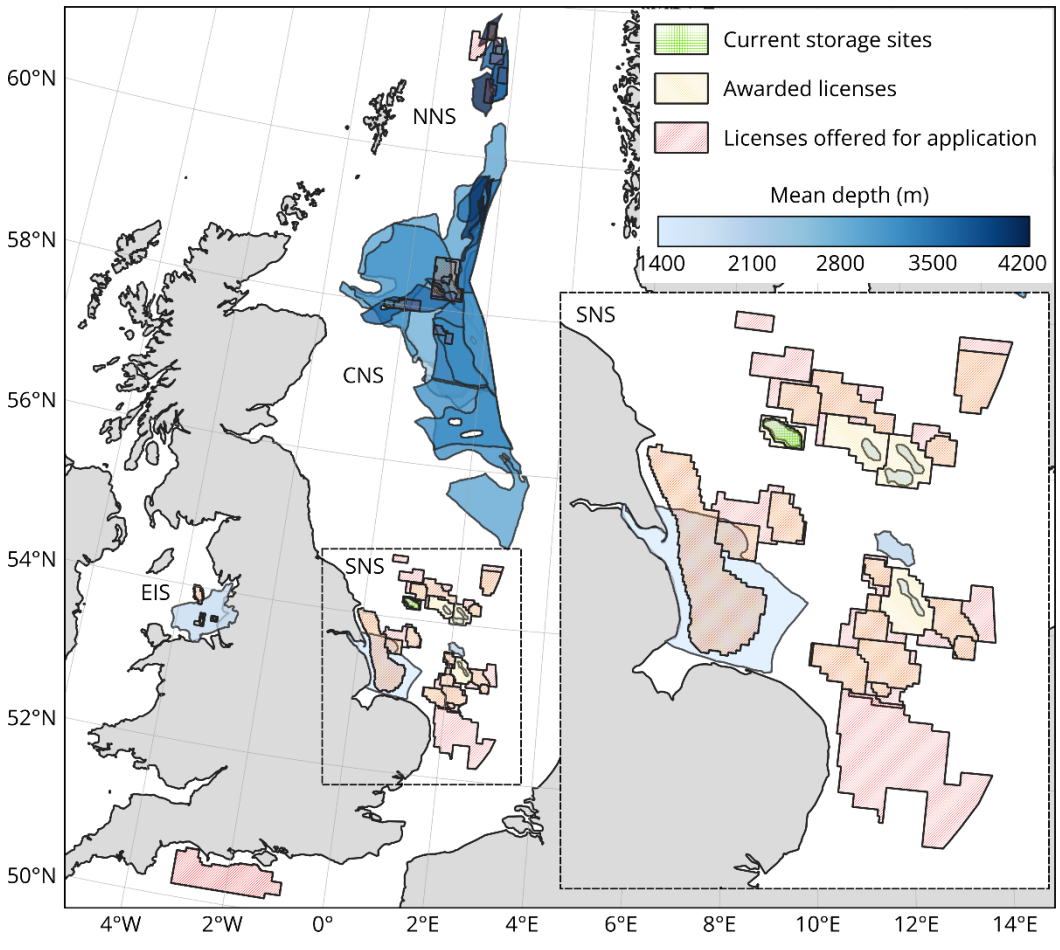

Fig. 3. Distribution of the UK offshore (EIS: East Irish Sea, SNS, CNS, and NNS: Southern, Central, and Northern North Sea, respectively) saline aquifers for geological CO_2 storage together with current storage sites, awarded licenses, and licenses offered for application. The inset shows the distribution of resources and licenses in the southern North Sea. Note that the geographically overlapping saline aquifers in the central and northern North Sea belong to different stratigraphic layers. Storage unit outlines are manually digitised from the CO_2Stored web viewer and represent approximate extents for illustrative purposes only

3. Results

3.1. Growth model projections of CO_2 storage in the UK

Constraining both logistic and Gompertz models to the UK storage resource of 78 Gt and to mid-century injection targets of 75, 130, and 175 Mt yr^{-1} shows that 2050 lies within an early growth stage rather than near saturation of the resource base (Fig. 4). To meet these targets, cumulative storage must increase at average annual rates of 5.8–9.2% between 2030 and the inflection year, and the cumulative storage used by 2050 is low relative to the resource base. The logistic pathways yield 1.15–1.93 Gt resource used by mid-century, while the Gompertz pathways yield 1.25–2.23 Gt. These values correspond to only 1.5–2.9% of the total 78 Gt storage resource.

This can be understood more clearly by considering the positions of the inflection year and the peak year in the growth models relative to the geological resource base. These points are fixed by the geometry of each model family and do not depend on the chosen 2050 target. For the logistic model, the inflection occurs at around 21% total geological capacity, equivalent to 16.5 Gt, and the peak rate coincides with the consumption of exactly half the resource at 39.0 Gt. For the Gompertz model, the corresponding values are much earlier in cumulative resource use, with 5.7 Gt for the inflection year, after storing roughly one-third of the cumulative mass required to reach the inflection year in the logistic model, and 28.7 Gt for the peak year. In other words, the Gompertz trajectory reaches both inflection and peak after a substantially smaller fraction of the total resource has been used. This difference arises from the intrinsic asymmetry of the Gompertz form and is the main reason why the two model families diverge so strongly after 2050.

These geometric anchors also translate into different temporal and intensity profiles for the scaleup. In the logistic family, the interval between inflection and peak is short, only 14–

20 years. In the Gompertz family, the same interval extends to 44–66 years, roughly 3 times longer. This produces a marked contrast in peak-rate requirements. Logistic pathways reach peak injection rates of 1.29-1.81 Gt yr^{-1}, an order of magnitude larger than the 2050 target. Gompertz pathways peak at only 0.42-0.63 Gt yr^{-1}, about 3.6-5.6 times the corresponding 2050 target. For the most ambitious 175 Mt yr^{-1} scenario, the logistic peak reaches 1.81 Gt yr^{-1}, compared with 0.63 Gt yr^{-1} for the Gompertz case, for the same 2050 rate target and converge to the same ultimate storage resource. The choice of growth model, therefore, has major consequences for the peak injection rate, and this in turn has an impact on the evaluation of the dynamic geophysical limits. A later inflection, as in the logistic case, concentrates the burden of scaleup into a shorter period and drives much higher peak injection demand. An earlier inflection, as in the Gompertz case, distributes that burden over a longer time window and lowers the required peak rate.

The significance of inflection year for near-term planning is most evident when comparing its timing relative to 2050, where we have imposed the rate constraint. Across all six scenarios, the inflection year falls between 2064 and 2094, placing 2050 some 14-44 years before the end of the strongly accelerating phase. By 2050, only 7-12% of the cumulative storage required to reach the inflection year has been delivered in the logistic cases, compared with 22-39% in the Gompertz cases.

Thus, mid-century policy targets do not probe the ultimate capacity of the UK subsurface. Rather, they test how rapidly the sector can progress through the early part of a much longer scaleup pathway. This point is important for the analysis that follows, because the geophysical challenge is not whether the UK can accommodate storage by 2050, but whether the much larger post-inflection injection rates implied by different growth trajectories remain compatible with subsurface injectivity limits.

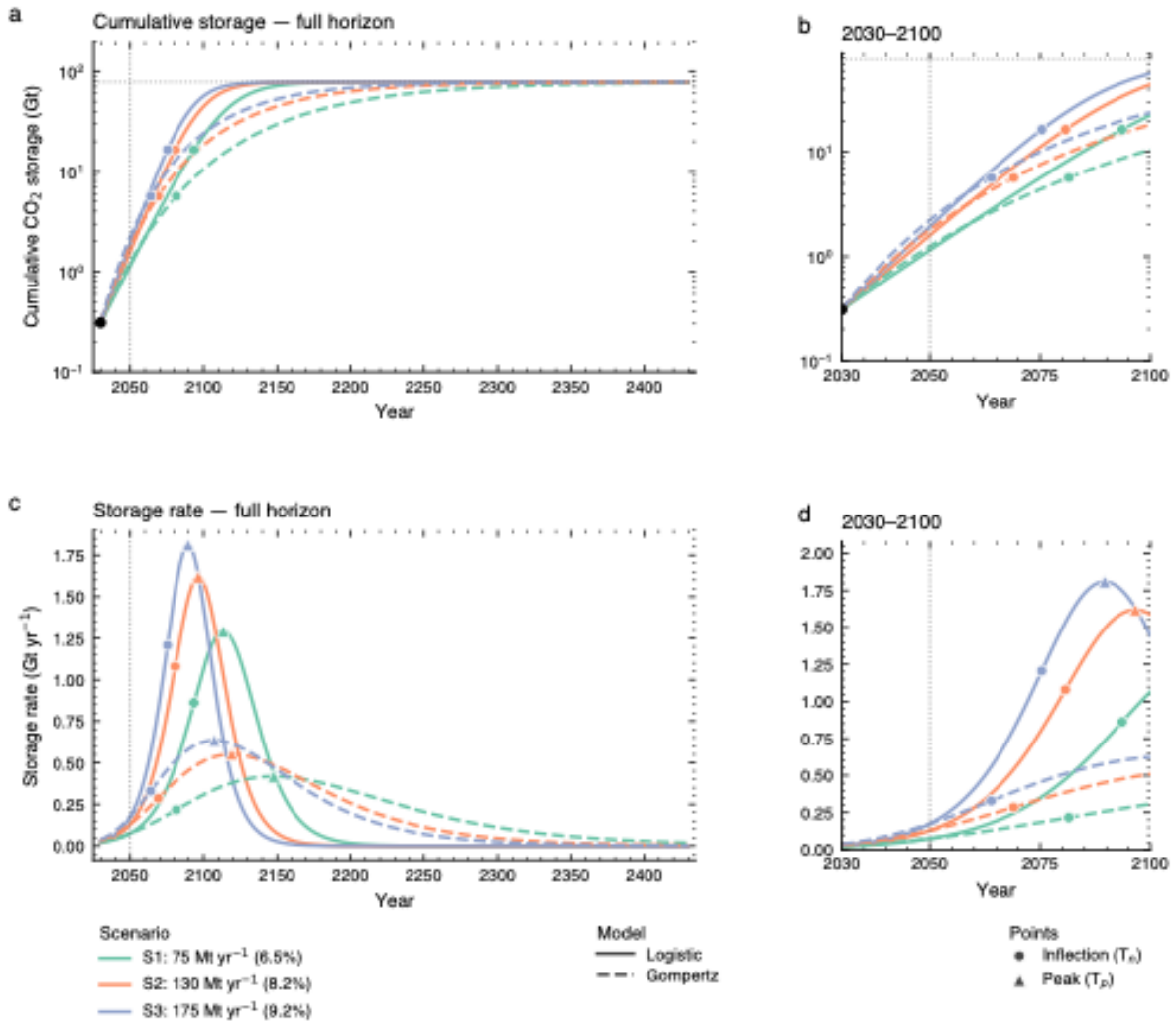

Fig. 4. Geological CO_2 storage scale-up trajectories for the United Kingdom generated using logistic and Gompertz growth models. Panels (a) and (c) show cumulative storage and annual injection rate over the full model horizon (2030–2430), while panels (b) and (d) show the corresponding trajectories for 2030–2100. For each model family, three 2050 injection-rate targets are considered: 75 Mt yr^{-1} (S1), 130 Mt yr^{-1} (S2), and 175 Mt y^{-1} (S3). Legend labels report the 2050 target rate together with the compound annual growth rate of cumulative storage between 2030 and the inflection year. Vertical dotted lines mark 2050, and the horizontal dotted line in panels (a) and (b) denotes the assumed 78 Gt geological storage capacity.

3.2. Injectivity limited resources of the UK offshore

The total storage capacity provided by the 27 storage units selected in this study approaches 79 over a 100-year injection period, corresponding to a regional injection rate of 790 Mt yr^{-1}. Detailed injectivity calculations, optimisation of injection-site configurations, and storage capacity estimates of all units are detailed in §S3 of the Supporting Information. Nearly 630 injection sites are required to achieve this rate (Table S1). The largest contributions come from Mey 5 and Maureen 2 with 28.5 and 14 Gt storage capacities in the central and northern North Sea, respectively (Fig. 5). These large capacities reflect their considerable areal extent, thickness, and permeability, favourable stress conditions and open boundary flow regimes. Indeed, while units with open boundary flow conditions constitute only one quarter of the considered storage units, they provide more nearly 70% of the total storage capacity. Contributions from confined units are dominated by Cormorant 009 18 in the northern North Sea and Collyhurst SS Fm 1 in the East Irish Sea, which together offer an additional ~12 Gt of cumulative storage resource.

In contrast, several storage units can not withstand pressure buildup associated with injection rates above the minimum threshold of 1 Mt yr^{-1} even through one injection site. Their effective storage capacities therefore fall below the minimum viable level and are excluded from the analysis here (capacities denoted by "-" in Table S1). These units include several small Bunter Closures in the southern North Sea. Overall, the southern, central, and northern North Sea and East Irish Sea account for approximately 7%, 56%, 31%, and 6%, respectively, of the total estimated UK offshore storage resources (Fig. 5). The obtained results underscore the substantial storage potential of the central and northern North Sea regions and highlight their critical role in meeting national CO_2 storage scaleup trajectories.

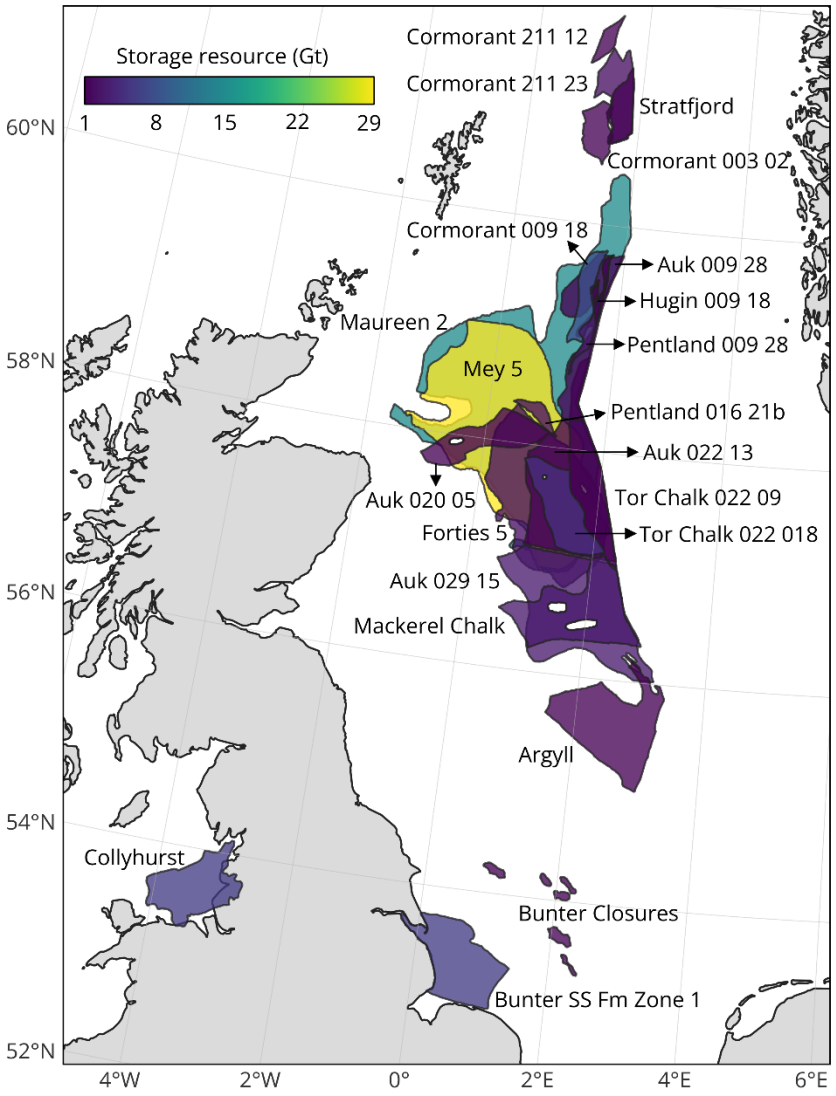

Fig. 5. Spatial distribution of CO_2 storage resources in the UK offshore saline aquifer calculated for 100 years of continuous injection at constant rates.

3.3. Injectivity limits to CO_2 storage scaleup

3.3.1. Logistic growth trajectories

The resource allocation analysis shows that the logistic growth trajectories targeting CO_2 storage rates of 75, 130 and 175 Mt yr^{-1} by 2050 and a cumulative storage amount of 78 Gt cannot be fully accommodated within the assessed UK offshore storage units (Fig. 6).

Although sufficient storage resources exist to accommodate these cumulative storage targets (§3.1), the peak injection rates implied by the growth models exceed the aggregate injectivity of the available storage units. This observation is independent of the resource allocation sequence, although the allocation strategy that prioritises smaller-capacity units accommodates slightly lower peak injection rates and cumulative storage amounts than the strategy prioritising larger units (compare Figs. 6a and 6b). The observed trend indicates that the limiting factor for these trajectories is the achievable injection rate rather than the total storage resource.

Having now identified that the growth trajectories cannot be achieved due to dynamic geophysical limits (reservoir pressurisation), the modelling framework updates the growth trajectory to a path that can be achieved without overpressuring the system. Lowering the peak injection rate in a logistic curve while maintaining the starting point and 2050 rate targets has the impact of reducing the total storage resource. A growth trajectory with a 2050 storage rate of 175 Mt yr^{-1} (the most aggressive target 2050 rate considered in this study), with a corresponding peak injection rate of approximately 1.6 Gt yr^{-1} results in a cumulative storage amount of 69 Gt (Fig. 7).

An important outcome of this modelling framework is the ability to identify the storage resource base that can be used along feasible growth trajectories, under dynamic geophysical constraints. Identifying a resource base of 69 Gt, for example, suggests that there is some risk that the 78 Gt represents an overestimate of the storage resource base relative to what can be achieved under growth and geophysical constraints. However, as will also be discussed below, ultimately the 78 Gt estimate falls well within the resulting range of outcomes emerging from the exploration of uncertainty in parameters.

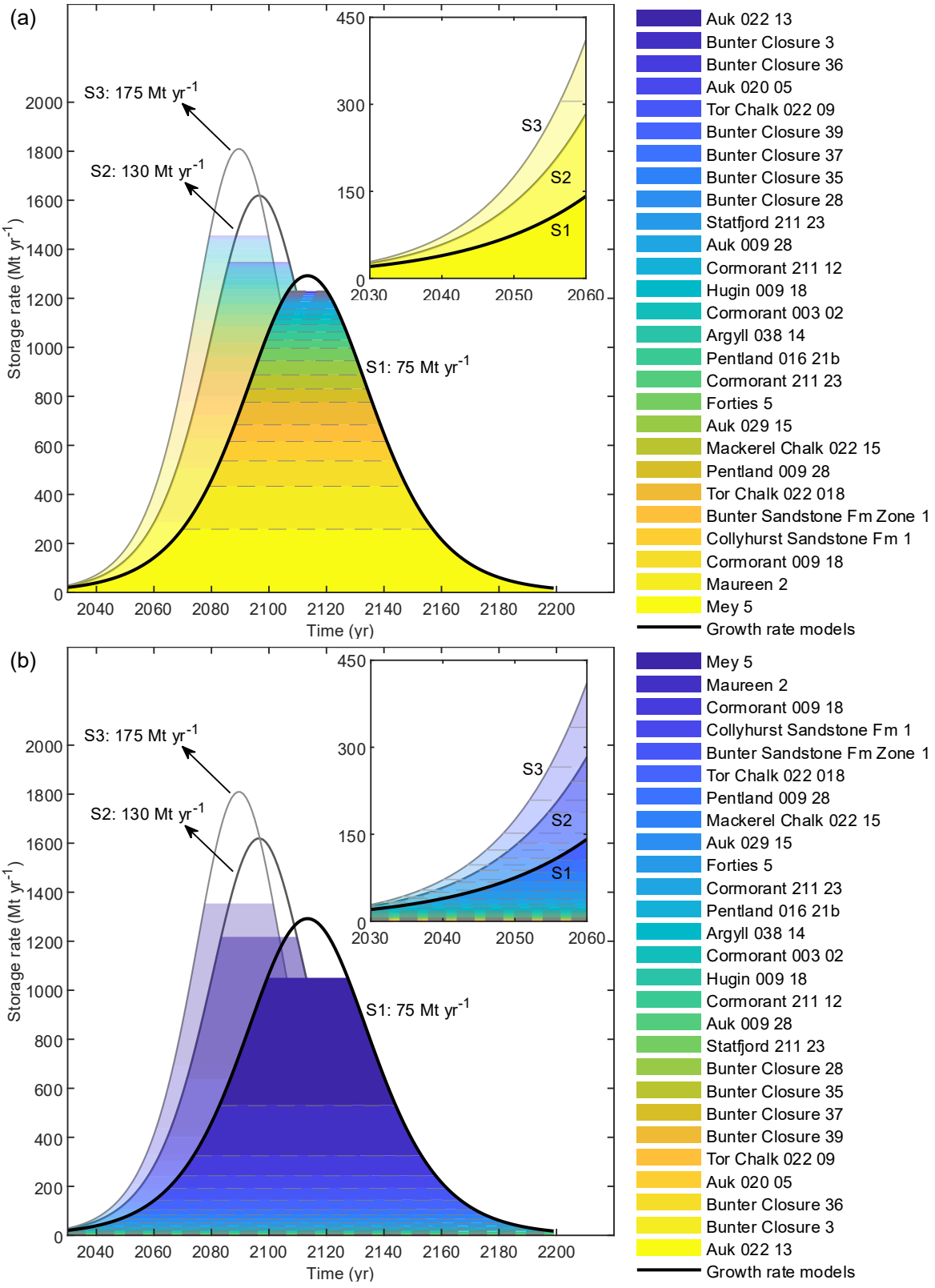

Fig. 6. Screening allocation of resources in (a) descending and (b) ascending order of capacity, under reservoir injectivity constraints, for three growth rate models targeting CO_2 storage rates

of 75 Mt yr^{-1} (S1), 130 Mt yr^{-1} (S2), and 175 Mt yr^{-1} (S3) by 2050 and a cumulative storage resource of 78 Gt. Insets show zoomed views of the plots during the early stages of injection.

The second end-member allocation scenario, prioritising the smallest storage units, still allows this scaleup trajectory without meeting geophysical limitations, although this allocation scenario would be more resource-intensive (Fig. S7). Twenty storage units would be needed to accommodate the scaleup to 2050, and all of the storage units would be needed to accommodate trajectory across the entirety of the logistic trajectory. The reason for the observed differences between the two resource allocation strategies is mainly twofold. First, several small units considered for long-duration injection can not tolerate large injection rates and therefore contribute only marginally to the cumulative storage amount. Second, assigning large-capacity units with open flow boundary regimes like Mey 5 and Maureen 2 to elongated injections is advantageous because sufficient time is provided for part of the excess pressure to dissipate at boundaries, slightly expanding the storage capacity.

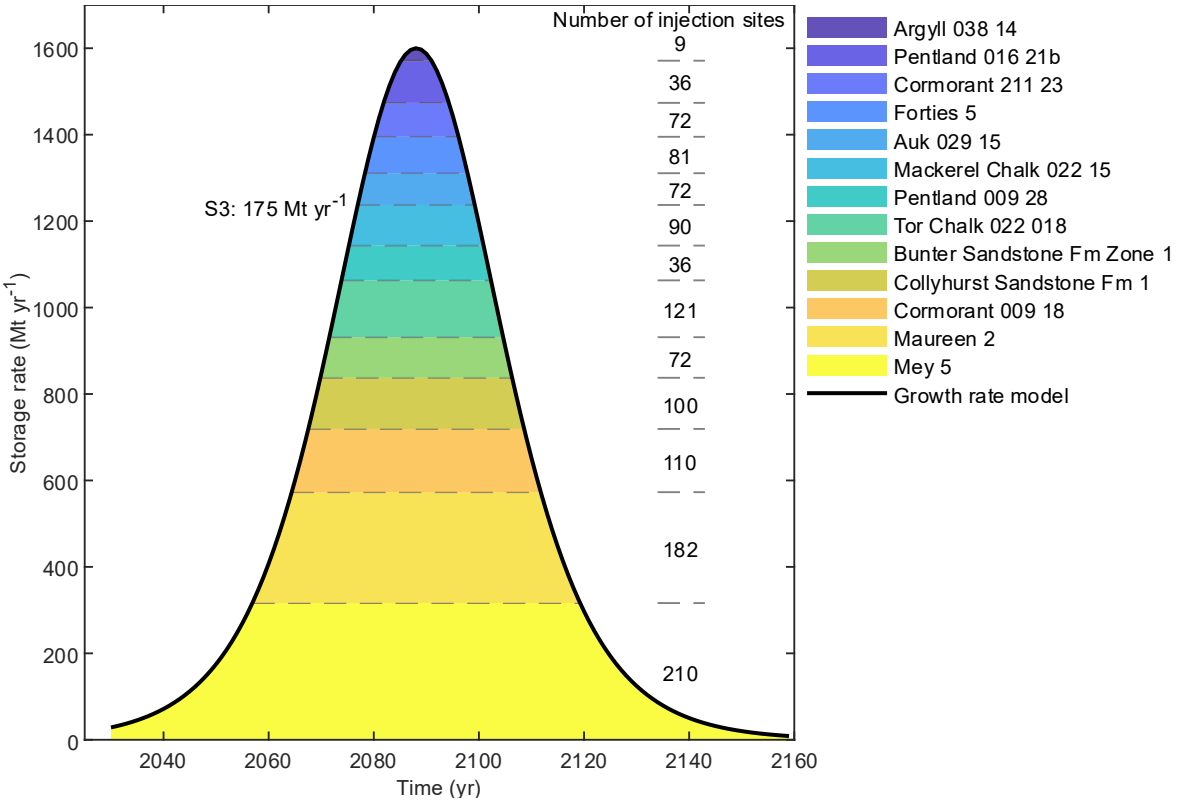

Fig. 7. Resource allocation under the growth rate model targeting a 2050 storage rate of 175 Mt yr^{-1} and a cumulative storage amount of 69 Gt, for the scenario prioritising the largest units.

Analysis of 100 random allocation scenarios shows that the majority of scenarios are capable of addressing the Q_{2050} = 175 Mt yr^{-1} target and a cumulative storage amount of 69 Gt (Fig. 8). Only three scenarios marginally fail to meet this target. The required number of geological units varies with the allocation sequence but remains within the range defined by the two allocation strategies described above. This trend supports the interpretation that these resource allocation strategies represent end-member cases. Consequently, any realistic allocation pathway lying between these extremes would be sufficient to meet the projected scaleup trajectory.

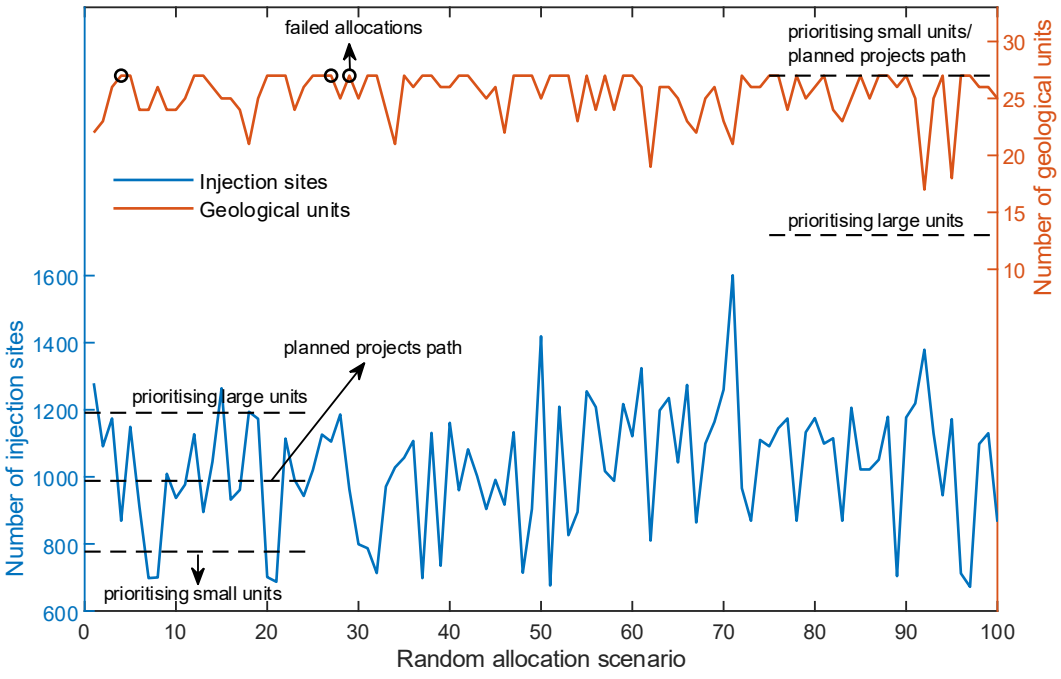

Fig. 8. Number of injection sites (left axis) and geological units (right axis) across random allocation scenarios. Horizontal dashed lines indicate key allocation strategies, including prioritisation of large units, prioritisation of small units, and the scenario consistent with the planned projects pathway.

A plausible allocation sequence consistent with currently planned CO_2 storage developments prioritises the southern North Sea, the East Irish Sea, the central North Sea and the northern North Sea. The results indicate that this allocation pathway can also accommodate growth trajectories with a storage resource base of 69 Gt (Fig. S8), further demonstrating that the conclusion is largely independent of the specific order in which storage resources are developed. Furthermore, the demonstrated ability to allocate resources for the most aggressive growth rate model achieving 175 Mt yr^{-1} injection rate by 2050 means that any other considered trajectory with a smaller 2050 target injection rate but similar cumulative storage mass can be safely addressed.

The resource allocation analysis highlights the extensive infrastructure requirements associated with large-scale CO_2 storage deployment. Approximately 210 injection sites within the Mey 5 unit are needed once the full injection rate of 300 Mt yr^{-1} is attained. However, achieving the peak injection rates projected by logistic growth models necessitates a much larger number of injection sites for optimized use of the storage resources. At its peak rate of 1.6 Gt yr^{-1}, nearly 1,200 injection sites are needed under the reference resource allocation approach, i.e., prioritising larger units (Fig. 7). This high demand implies the combined effects of long injection durations, the imposed technological upper limit of 20 Mt yr^{-1} per site, and local injectivity constraints associated with unfavourable reservoir properties. The latter factor is exemplified by the Tor Chalk 022 018 unit, where a reservoir permeability of only 5 mD entails use of 121 injection sites to maximize its contribution to addressing the scaleup trajectories (Fig. 7).

The total number of injection sites across 100 random resource allocation scenarios ranges from approximately 700 to nearly 1,600 (Fig. 8). The first allocation scenario lies toward the upper bound of this range, whereas the conservative allocation strategy, i.e., prioritising small-capacity units, with 780 injection sites, and the sequence consistent with currently

planned projects, with 990 injection sites, lie close to the lower bound and the mean of the distribution, respectively (Fig. 8). This variability occurs because the number of sites deployed within each storage unit differs substantially between scenarios, primarily as a function of injection duration. In particular, large-capacity units assigned to long injection periods under the first allocation strategy require a larger number of injection sites operating at relatively low rates to maximise storage utilisation. In contrast, when these units are allocated later in the sequence and over shorter injection periods in the second allocation strategy, fewer sites operating at higher injection rates are sufficient to achieve the required storage contribution. As such, the framework optimises injection grid design to maximise total injectivity and cumulative storage capacity, rather than to minimise the number of injection sites, and the resulting site counts emerge as a secondary outcome of this optimisation.

Reducing the maximum number of injection sites in each geological unit, based on the historical number of hydrocarbon wells drilled in the corresponding region, imposes an additional constraint on storage deployment. This decreases the maximum attainable peak injection rate to approximately 1.5 Gt yr^{-1} and the cumulative storage amount to 64 Gt (Fig. S9). The Mey 5 and Maureen 2 units are exceptions, as their contribution to the growth trajectories remains unaffected owing to the large number of existing wellbores (Fig. S9). In contrast, Tor Chalk 022 018 is no longer among the major contributing storage units because of the limited historical drilling activity in this region combined with its relatively low injectivity. In this setting, nearly 880 injection sites are still sufficient to achieve the target storage rate of 175 Mt yr^{-1} by 2050 with the lowered associated storage resource base of 64 Gt.

3.3.2. Gompertz growth trajectories

In contrast to the logistic growth models, the Gompertz growth model fully accommodates the scaleup pathway targeting a storage rate of 175 Mt yr^{-1} by 2050 and a

cumulative storage amount of 78 Gt (Fig. 9). This difference arises from the slower growth and decline phases of the Gompertz model, which reduce the peak injection rate to approximately 640 Mt yr^{-1}. The combination of longer injection durations and lower peak rates reduces pressure interference between injection sites and allows for more sustainable and efficient utilisation of storage resources. In particular, the elongated injection strategy substantially increases the contribution of Mey 5 (~41 Gt) relative to the logistic growth trajectories (~27 Gt) (compare Figs. 9 and 7), as its high injectivity and open boundary conditions allow pressure dissipation over long injection durations. Consequently, a larger fraction of the total storage resource can be accommodated within a small number of highly favourable storage units.

The reduced peak injection rate without substantial loss of per-site injectivity is translated into a smaller number of required injection sites under Gompertz trajectories. While the logistic growth trajectory with a storage resource of C = 69 Gt requires approximately 1200 injection sites under the reference allocation strategy (Fig. 7), the Gompertz trajectory with the storage resource C = 78 Gt can be achieved using only 477 injection sites (Fig. 9). This reduction demonstrates the strong dependence of storage deployment requirements on the assumed growth trajaectory, and corresponding temporal evolution of injection rates.

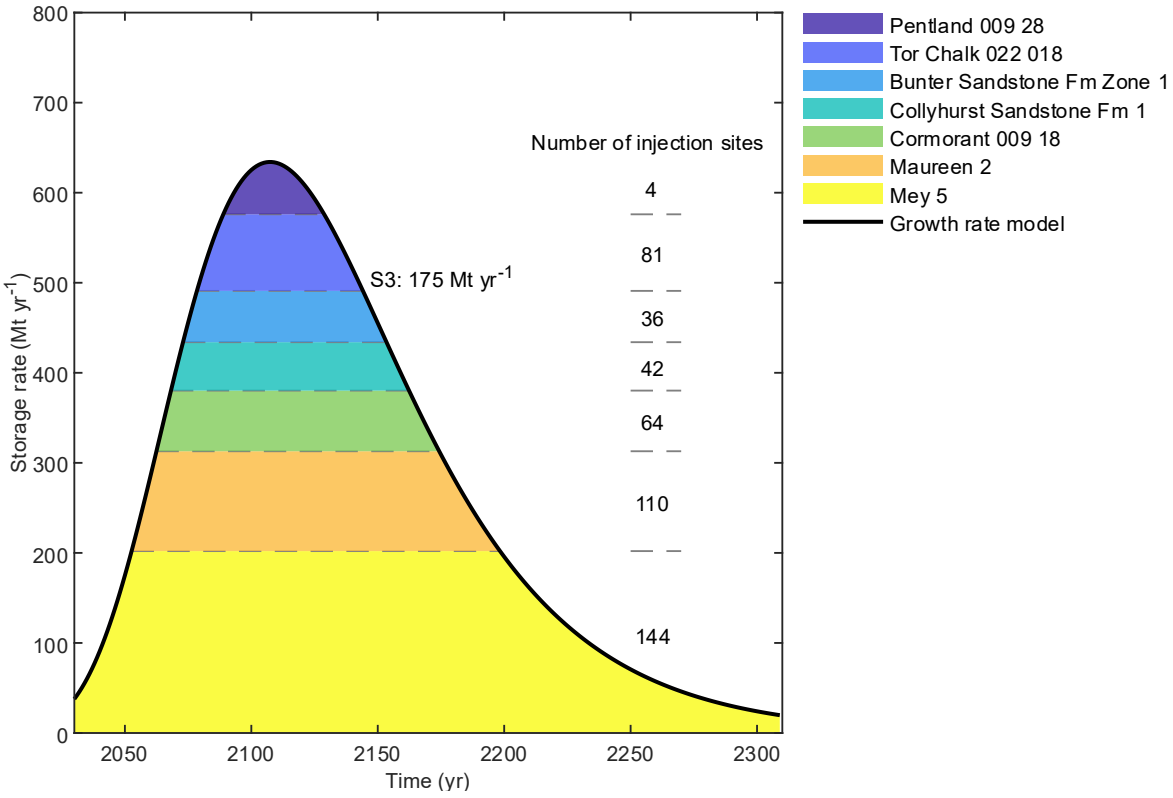

Fig. 9. Resource allocation for the Gompertz model targeting a CO_2 storage rate of 175 Mt yr^{-1} by 2050 and a cumulative storage mass of 78 Gt. Note that the scales are different from the plots for the growth rate model.

3.3.3. Impact of uncertainties in reservoir permeability

The obtained results so far are based on reservoir pressurisation models parameterised using the most likely hydraulic properties reported in the CO_2Stored database. When uncertainty is introduced in reservoir permeability, the 2050 targets can still be met, but the long-term scaleup trajectories discussed so far become increasingly difficult to sustain. As permeability decreases, pressure limitations become progressively more restrictive, reducing both the peak injection rates and cumulative storage amounts that can be attained. This effect is evident for the Gompertz trajectories targeting a 2050 storage rate of 175 Mt yr^{-1} (Fig. S10). While this trajectory can be achieved with a total storage resource of 78 Gt under the reference permeability values, a tenfold reduction in permeability precludes achieving the required peak

injection rates due to pressure constraints, reducing the achievable storage resource base from 78 to 41 Gt. In all cases of reduced permeability by factors from 2 to 10, the achievable storage resource base is reduced from 78 Gt (Fig. 10).

As previously described, imposing lower peak injection rates while maintaining a storage rate in 2050 is equivalent to reducing the storage resource base in the growth models. We thus use this modelling framework to identify the sensitivity of the achievable storage resource base to uncertainty. We generate alternative trajectories by lowering the maximum allowable peak injection rate in steps of 50 Mt yr^{-1} and 40 Mt yr^{-1} relative to the reference cases for logistic and Gompertz trajectories, respectively, while maintaining Q_{2050}. The resulting trends show a non-linear decrease in the achievable storage resourece base with decreasing permeability (Fig. 10). For logistic trajectories, even a twofold reduction in permeability ($k/2$) leads to a marked reduction in both peak injection rates and achievable storage resource (Fig. 10a). A tenfold permeability reduction ($k/10$) reduces the attainable peak injection rates by ~600 Mt yr^{-1} and the cumulative storage amount by ~30 Gt relative to the reference case. Within Gompertz trajectories, achievable injection rates decrease more gradually with permeability reduction owing to their lower peak injection rates and more uniformly across the injection duration (Fig. 10b). As a result, the reduction in cumulative storage remains comparable to, and in some cases exceeds, that observed for logistic trajectories. Thus, although Gompertz trajectories are less constrained by peak-rate reductions, their ultimate cumulative storage remain sensitive to permeability uncertainty. Yet, substantial deployment including all Q_{2050} targets remain achievable even under severe reductions in permeability.

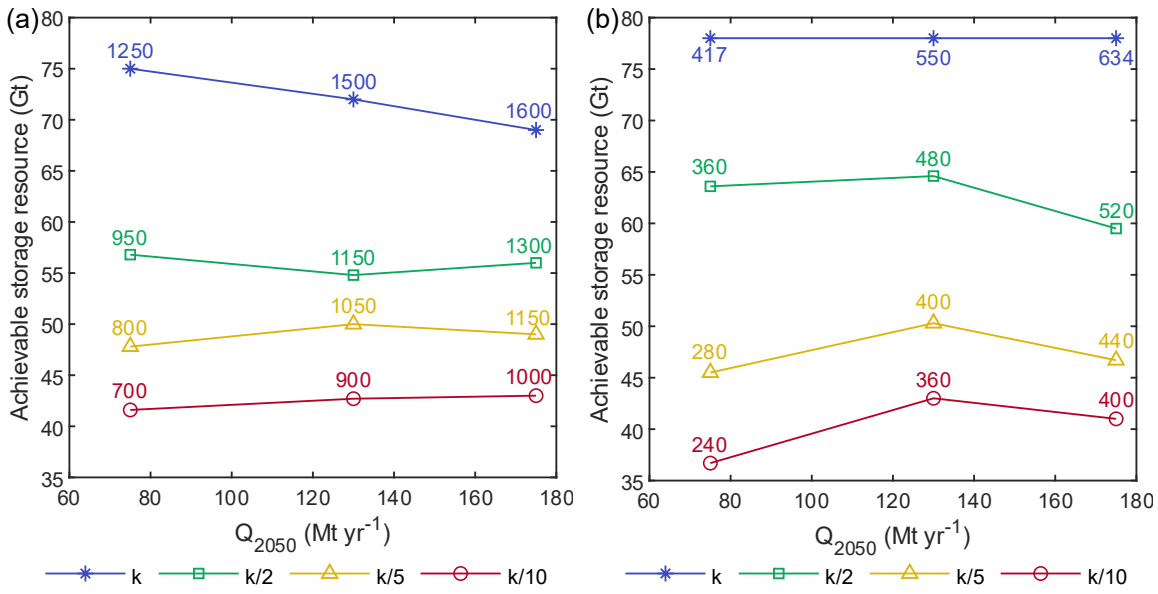

Fig. 10. Estimated achievable storage resource for (a) logistic and (b) Gompertz growth trajectories targeting 75, 130, and 175 Mt yr^{-1} by 2050, considering uncertainties in reservoir permeability: most likely permeabiliy values from the CO_2Stored databased (k) and reduced by factors of 2 ($k/2$), 5 ($k/5$), and 10 ($k/10$). The corresponding peak injection rates (Mt yr^{-1}) for each scenario are shown as labels.

4. Discussion

Our analysis shows that CO_2 storage scaleup trajectories considered for the UK can be accommodated without exceeding critical geophysical limits. Even under severe reductions in reservoir permeability, all UK government mid-century deployment targets, including achieving storage rates of 175 Mt yr^{-1}, remain feasible. However, reservoir pressurisation imposes meaningful constraints on the pace and ultimate scale of storage deployment. Thus, while reservoir pressurisation is unlikely to constrain the achievement of national-scale mid-century targets, it may limit the long-term growth and cumulative storage that can ultimately be attained. Instead, the primary limiting factor emerges from the achievable pace of industrial expansion to meet climate change mitigation roadmaps.

The ability of UK offshore saline aquifers to accommodate aggressive CO_2 storage growth trajectories is underpinned by the large dynamic storage resources estimated in this study, which approach 79 Gt when assuming injection at a constant, sustainable rate over a century. This estimate exceeds the pressure-limited storage capacity of approximately 22 Gt derived by de Jonge-Anderson et al. (2026),[38] is moderately higher than the ~71 Gt estimated by Smith et al. (2024),[54] and remains below the ~140 Gt reported by De Simone and Krevor (2021).[36] The discrepancies likely reflect differences in geological representation and modelling assumptions. de Jonge-Anderson et al. (2026)[38] and Smith et al. (2024)[54] employed the spatially coarse-resolution GSEU[53] and global sedimentary[55] databases, both excluding the overlapping storage units and assuming closed boundary flow conditions. In contrast, the more detailed representation of geological units adopted here suggests open-flow boundary conditions for a number of aquifers, enabling lateral pressure dissipation and increasing accessible pore space. Additionally, the use of refined geophysical parameters, particularly field-constrained estimates of in situ stress and effective rock compressibility further contributes to the larger storage resources estimates. Although De Simone and Krevor (2021)[36] employed a similar geological database (CO_2Stored database), the lower estimates obtained here is primarily because of the use of region-specific geomechanical constraints, the application of a minimum technical injection-rate threshold for site development, and improvements to CO2BLOCK-GROWTH for closed-boundary pressure buildup calculations.

We show that reaching Gt-scale injection rates outlined by growth rate models requires up to ~1,600 injection sites (Fig. 8), depending on the scaleup trajectory and resource allocation strategy. This corresponds to approximately 4,800 injection wellbores assuming three wells per site. This scale of deployment is consistent with previous regional and global assessments. At the UK scale, de Jonge-Anderson et al. (2026)[38] highlight the need for nearly 800 injection wellbores for storage scaleup to 300 Mt yr^{-1} by 2050. Ringrose and Meckel (2019)[25] also

suggest that achieving the IEA[56] projected ~7 Gt yr^{-1} of CO_2 storage by 2050 would require around 10,000 injection wells worldwide. Although these numbers may appear large, they are not unprecedented. Over six decades of hydrocarbon exploration and production, the UK continental shelf has cumulatively hosted more than 13,000 offshore wellbores with peak drilling activity exceeding 400 wells per year.[46] Nearly 6,000 wells have penetrated candidate UK offshore storage aquifers, still exceeding the number required to meet the projected growth trajectories. This level of historical subsurface development in terms of offshore engineering, logistic and regulatory capabilities needed to deliver high-density well networks renders achieving national CO_2 storage scaleup targets technically plausible.

A further technoeconomic consideration arises from the fact that the storage units providing the largest contributions, particularly in the central and northern North Sea, involve deep formations, often exceeding 2.5 km depth. These depths may offer enhanced CO_2 containment underground by (1) promoting residual and dissolution trapping mechanisms, particularly, in thick and dipping formations,[57] (2) enhancing the likelihood of forming secondary CO_2 accumulations in multilayered sedimentary settings,[58,59] and (3) increasing mechanical stability by elevating tensile failure limits of the caprock.[36] They also reduce upward pressure propagation toward shallow groundwater.[60] However, well construction and operational costs may significantly increase with depth.[61] Consequently, despite excellent injectivity and capacity offered by these deep units, their development entails sustained investment and supportive policy frameworks. Therefore, the UK's largest storage resources are technically available but economically demanding.

Our resource-allocation framework assumes that all injection sites assigned to a given unit are available from the beginning of its operational period. In reality, CO_2 storage development will follow a sequential progress, beginning with a small number of hubs and expanding over time as the infrastructure, permitting, and transport networks become mature.

This phasing should still not compromise reservoir injectivity as injection rates remain far below critical thresholds. However, our analysis indicates that the largest regional storage rates are achieved through dense grids of injectors operating at relatively low per-site rates. While a smaller number of high-rate injectors can deliver comparable cumulative rates, they may delay the ramp-up of national storage rates and pose difficulty in reaching more ambitious mid-century targets. The initial gradual rise in storage rates can be compensated for by elongating the high-injection period, which is also compatible with geophysical limits, as it allows for more sustainable use of the subsurface resources. Such scaleup profiles may represent more realistic trajectories for achieving ambitious UK-wide CO_2 storage goals.

Our analysis adopts regular, uniform site patterns within each storage unit, yielding conservative estimates of pressure interferences. In practice, well placement can be optimised to address geological heterogeneities and minimise reservoir pressurisation.[62] Basin-scale pressure management strategies, such as brine extraction or coordinated operation across neighbouring units, could further reduce pressure buildup and unlock additional storage capacity.[63,64] This suggests that our estimates of injectivity and storage capacity represent lower bounds on what could ultimately be achieved under optimised operations. Such site- and field-level development strategies warrant detailed subsurface characterisation and high-resolution, multiphysics simulations that acknowledge subsurface structural and physical complexities, which fall beyond our screening-level study.

Despite remaining geophysical uncertainties and methodological simplifications, the conducted sensitivity analyses suggest that the key conclusions of this study remain robust. substantial UK CO_2 storage scaleup trajectories remain feasible within geophysical constraints, suggesting that large-scale deployment will primarily depend on the ability to sustain the required industrial, infrastructural, and investment growth. This indicates that the UK's offshore storage resources are sufficient to support large-scale decarbonisation, provided that

policy, investment, and industrial capacity expand at a pace consistent with national climate commitments. More broadly, the framework developed in this study is transferable to other national and regional contexts, thereby supporting the assessment of CO_2 scaleup feasibility globally. The incorporation of this framework into integrated assessment models would enable a more realistic representation of the timing, scale, and physical limits of subsurface storage in long-term decarbonisation pathways.

Acknowledgements

I.R.K., X.G. and S.K. acknowledge funding through a Senior Research Fellowship jointly funded by Shell and the Royal Academy of Engineering (RCSRF2223-1677). I.R.K. and S.K. also acknowledge funding from the Engineering and Physical Sciences Research Council through the UKRI Postdoc Guarantee Award THMC4CCS (Grant number EP/X026019/1). I.R.K. also acknowledges funding from MICIU/AEI /10.13039/501100011033 and from the FSE+ through the 'Ramón y Cajal' fellowship (reference RYC2024-048711-I).

Data availability statement

The scripts for the CO2BLOCK-GROWTH tool, along with the input files used for resource estimates and allocations in the UK CO_2 storage scaleup study, are publicly available at https://github.com/ImperialCollegeLondon/CO2BLOCK/.

References

(1) IPCC, 2018. Global Warming of 1.5 ºC. An IPCC Special Report on the impacts of global warming of 1.5 ºC above pre-industrial levels and related global greenhouse gas

emission pathways, in the context of strengthening the global response to the threat of climate change, sustainable development, and efforts to eradicate poverty, ed. Masson-Delmotte, V. et al.

(2) IPCC, 2022. Climate change 2022: Mitigation of climate change. Contribution of working group III to the sixth assessment report of the Intergovernmental Panel on Climate Change, ed. Shukla, P.R. et al.

(3) Luderer, G., et al., 2015. Description of the REMIND model (Version 1.6). Available at SSRN: https://ssrn.com/abstract=2697070.

(4) Shell, 2018. Sky Scenario. Available at: https://www.shell.com/energyand-innovation/the-energy-future/scenarios/what-are-theprevious-shell-scenarios/shell-scenario-sky.html.

(5) Stehfest, E., van Vuuren, D., Bouwman, L., Kram, T., 2014. Integrated assessment of global environmental change with IMAGE 3.0: Model description and policy applications. Netherlands Environmental Assessment Agency (PBL).

(6) UK Government, 2023a. Carbon capture, usage and storage: a vision to establish a competitive market. https://www.gov.uk/government/publications/carbon-capture-usage-and-storage-a-vision-to-establish-a-competitive-market/carbon-capture-usage-and-storage-a-vision-to-establish-a-competitive-market

(7) Zhang, Y., Jackson, C., Zahasky, C., Nadhira, A., Krevor, S., 2022. European carbon storage resource requirements of climate change mitigation targets. Int J Greenhouse Gas Control 114, 103568. https://doi.org/10.1016/j.ijggc.2021.103568

(8) North Sea Transition Authority (NSTA), 2023a. UK oil and gas reserves and resources. Available at: https://www.nstauthority.co.uk/news-publications/publications/.

(9) McFarland, J.R., Herzog, H.J., 2006. Incorporating carbon capture and storage technologies in integrated assessment models. Energy Econ. 28(5-6), 632-652. https://doi.org/10.1016/j.eneco.2006.05.016

(10) Vasylkivska, V., Dilmore, R., Lackey, G., Zhang, Y., King, S., Bacon, D., Chen, B., Mansoor, K., Harp, D., 2021. NRAP-open-IAM: A flexible open-source integrated-assessment-model for geologic carbon storage risk assessment and management. Environ. Modell. Software 143, 105114. https://doi.org/10.1016/j.envsoft.2021.105114

(11) Iyer, G., Hultman, N., Eom, J., McJeon, H., Patel, P. and Clarke, L., 2015. Diffusion of low-carbon technologies and the feasibility of long-term climate targets. Technol. Forecasting Social Change 90, 103-118. https://doi.org/10.1016/j.techfore.2013.08.025

(12) Bashir, A., Ali, M., Patil, S., Aljawad, M.S., Mahmoud, M., Al-Shehri, D., Hoteit, H., Kamal, M.S., 2024. Comprehensive review of CO_2 geological storage: Exploring principles, mechanisms, and prospects. Earth Sci. Rev. 249, 104672. https://doi.org/10.1016/j.earscirev.2023.104672

(13) Hendriks, C., Graus, W., van Bergen, F., 2004. Global carbon dioxide storage potential and costs. Utrecht, E. EEP-02001.

(14) Koelbl, B.S., van den Broek, M.A., Faaij, A.P. and van Vuuren, D.P., 2014. Uncertainty in carbon capture and storage (CCS) deployment projections: a cross-model comparison exercise. Clim. change 123(3), 461-476. https://doi.org/10.1007/s10584-013-1050-7

(15) Zhang, Y., Jackson, C., Krevor, S., 2024. The feasibility of reaching gigatonne scale CO_2 storage by mid-century. Nat. Commun. 15(1), 6913. https://doi.org/10.1038/s41467-024-51226-8

(16) Bachu, S., 2015. Review of CO2 storage efficiency in deep saline aquifers. Int. J. Greenhouse Gas Control 40, 188-202. https://doi.org/10.1016/j.ijggc.2015.01.007

(17) Szulczewski, M.L., MacMinn, C.W., Herzog, H.J., Juanes, R., 2012. Lifetime of carbon capture and storage as a climate-change mitigation technology. Proc. Natl. Acad. Sci. U.S.A. 109(14), 5185-5189. https://doi.org/10.1073/pnas.1115347109

(18) Kivi, I.R., De Simone, S., Krevor, S., 2025. A simplified physics model for estimating subsurface CO2 storage resources constrained by fault slip potential. J. Rock Mech. Geotech. Eng. 18(4), 2546-2560. https://doi.org/10.1016/j.jrmge.2025.06.031

(19) Zoback, M.D., Gorelick, S.M., 2012. Earthquake triggering and large-scale geologic storage of carbon dioxide. Proc. Natl. Acad. Sci. U.S.A. 109(26), 10164-10168. https://doi.org/10.1073/pnas.1202473109

(20) Alcalde, J., Flude, S., Wilkinson, M., Johnson, G., Edlmann, K., Bond, C.E., Scott, V., Gilfillan, S.M., Ogaya, X., Haszeldine, R.S., 2018. Estimating geological CO2 storage security to deliver on climate mitigation. Nat. Commun., 9(1), 2201. https://doi.org/10.1038/s41467-018-04423-1

(21) Celia, M.A., Bachu, S., Nordbotten, J.M., Gasda, S.E., Dahle, H.K., 2005. Quantitative estimation of CO2 leakage from geological storage: Analytical models, numerical models, and data needs. In Greenhouse Gas Control Technologies 7 (pp. 663-671). Elsevier Science Ltd.

(22) Fuhrman, J., Lane, J., McJeon, H., Iyer, G.C., Edwards, M.R., Thomas, Z., Edmonds, J.A., 2025. Rate and growth limits for carbon capture and storage. Environ. Res. Lett. 20(6), 064034. 10.1088/1748-9326/add9af

(23) Kazlou, T., Cherp, A., Jewell, J., 2024. Feasible deployment of carbon capture and storage and the requirements of climate targets. Nat. Clim. Change, 14(10), 1047-1055. https://doi.org/10.1038/s41558-024-02104-0

(24) Lane, J., Greig, C. and Garnett, A., 2021. Uncertain storage prospects create a conundrum for carbon capture and storage ambitions. Nat. Clim. Change 11(11), 925-936. https://doi.org/10.1038/s41558-021-01175-7

(25) Ringrose, P.S., Meckel, T.A., 2019. Maturing global CO2 storage resources on offshore continental margins to achieve 2DS emissions reductions. Sci. Rep. 9(1), 17944. https://doi.org/10.1038/s41598-019-54363-z

(26) Zahasky, C., Krevor, S., 2020. Global geologic carbon storage requirements of climate change mitigation scenarios. Energy Environ. Sci. 13(6), 1561-1567. 10.1039/D0EE00674B

(27) Brandt, A.R., 2007. Testing hubbert. Energy policy 35(5), 3074-3088. https://doi.org/10.1016/j.enpol.2006.11.004

(28) Gao, X., & Krevor, S. (2025). The London Register of Subsurface CO2 Storage: 2025 Annual Report. Imperial College London.

(29) Zhang, Y., Jackson, C. and Krevor, S., 2022. An Estimate of the Amount of Geological CO2 Storage over the Period of 1996–2020. Environ. Sci. Technol. Let. 9(8), 693-698. https://doi.org/10.1021/acs.estlett.2c00296

(30) Wilson, C., Grubler, A., Bauer, N., Krey, V., Riahi, K., 2013. Future capacity growth of energy technologies: are scenarios consistent with historical evidence?. Clim. Change 118(2), 381-395. https://doi.org/10.1007/s10584-012-0618-y

(31) Zhang, Y., Jackson, C., Darraj, N. and Krevor, S., 2023. Feasibility of carbon dioxide storage resource use within climate change mitigation scenarios for the United States. Environ. Sci. Technol. 57(40), 14938-14949. https://doi.org/10.1021/acs.est.3c00790

(32) Budinis, S., Krevor, S., Dowell, N.M., Brandon, N., Hawkes, A., 2018. An assessment of CCS costs, barriers and potential. Energy Strategy Rev. 22, 61-81. https://doi.org/10.1016/j.esr.2018.08.003

(33) Krevor, S., De Coninck, H., Gasda, S.E., Ghaleigh, N.S., de Gooyert, V., Hajibeygi, H., Juanes, R., Neufeld, J., Roberts, J.J., Swennenhuis, F., 2023. Subsurface carbon dioxide and hydrogen storage for a sustainable energy future. Nat. Rev. Earth Environ. 4(2), 102-118. https://doi.org/10.1038/s43017-022-00376-8

(34) Hubbert, M.K., 1956. Nuclear energy and the fossil fuels. Houston, TX: Shell Development Company, Exploration and Production Research Division. pp. 7-25.

(35) Rutledge, D., 2011. Estimating long-term world coal production with logit and probit transforms. Int. J. Coal Geol. 85(1), 23-33. http://dx.doi.org/10.1016/j.coal.2010.10.012

(36) De Simone, S. and Krevor, S., 2021. A tool for first order estimates and optimisation of dynamic storage resource capacity in saline aquifers. Int. J. Greenhouse Gas Control 106, 103258. https://doi.org/10.1016/j.ijggc.2021.103258

(37) Ganjdanesh, R., Hosseini, S.A., 2018. Development of an analytical simulation tool for storage capacity estimation of saline aquifers. Int. J. Greenhouse Gas Control, 74, 142-154. https://doi.org/10.1016/j.ijggc.2018.04.017

(38) de Jonge-Anderson, I., Johnson, G., Alcalde, J., Roberts, J.J., 2026. CO2LOGIX: A first-order model of pressure-constrained CO2 geological storage growth at the basin scale. Int. J. Greenhouse Gas Control 151, 104608. https://doi.org/10.1016/j.ijggc.2026.10460

(39) Hallock, J.L., Tharakan, P.J., Hall, C.A.S., Jefferson, M., Wu, W., 2004. Forecasting the limits to the availability and diversity of global convectional oil supply. Energy 29(11), 1673-1696. https://doi.org/10.1016/j.energy.2004.04.043

(40) Link, S., Schneider, L., Stephan, A., Weymann, L. and Plötz, P., 2025. Feasibility of meeting future battery demand via domestic cell production in Europe. Nat Energy 10, 526-534 (2025). https://doi.org/10.1038/s41560-025-01722-y

(41) Villanueva, D. and Feijóo, A., 2018. Comparison of logistic functions for modeling wind turbine power curves. Electr. Power Syst. Res. 155, 281-288. https://doi.org/10.1016/j.epsr.2017.10.028

(42) Global CCS Institute, 2025. Global status of CCS 2025. https://www.globalccsinstitute.com/global-status-of-ccs/

(43) UK Government, 2023b. CCUS Net Zero investment roadmap: Capturing carbon and a global opportunity. https://www.gov.uk/government/publications/carbon-capture-usage-and-storage-net-zero-investment-roadmap/ccus-net-zero-investment-roadmap-capturing-carbon-and-a-global-opportunity

(44) Stark, C., Thompson, M., Andrew, T., Beasley, G., Bellamy, O., Budden, P., Cole, C., et al. 2019. Net Zero: The UK's contribution to stopping global warming. UK Committee on Climate Change. https://www.theccc.org.uk/publication/net-zero-the-uks-contribution-to-stopping-global-warming/

(45) De Simone, S., Jackson, S.J., Krevor, S., 2019. The error in using superposition to estimate pressure during multisite subsurface CO2 storage. Geophys. Res. Lett. 46(12), 6525-6533. https://doi.org/10.1029/2019GL082738

(46) North Sea Transition Authority (NSTA), 2025. UK Drilling Activity. Excel data file. Accessed November 26, 2025. www.nstauthority.co.uk/data-and-insights/data/themes/wells/.

(47) North Sea Transition Authority (NSTA), 2023b. Net zero boost as carbon storage licences accepted. Available at: https://www.nstauthority.co.uk/news-publications/net-zero-boost-as-carbon-storage-licences-accepted/.

(48) Gibson-Poole, C.M., Taplin, M., Bouffin, N., Duffy, L., Sutherland, F., Cabral, A., Ashby, D., 2024. Site characterization of the endurance CO2 store, southern north sea, uk. Geoenergy, 2(1), geoenergy2024-012. https://doi.org/10.1144/geoenergy2024-012

(49) Smith, A., Hampson, G., Kivi, I.R., Krevor, S., 2025. Carbon dioxide plumes, pressure space and legacy well risk for Southern North Sea CO2 Storage Projects. Energy Geosci. 7(1), 100475. https://doi.org/10.1016/j.engeos.2025.100475

(50) Alcalde, J., Heinemann, N., Mabon, L., Worden, R.H., De Coninck, H., Robertson, H., Maver, M., et al. 2019. Acorn: Developing full-chain industrial carbon capture and storage in

a resource-and infrastructure-rich hydrocarbon province. J. Cleaner Prod. 233, 963-971. https://doi.org/10.1016/j.jclepro.2019.06.087

(51) Bentham, M., Mallows, T., Lowndes, J., Green, A., 2014. CO2 STORage evaluation database (CO2 Stored). The UK's online storage atlas. Energy Procedia, 63, 5103-5113. https://doi.org/10.1016/j.egypro.2014.11.540

(52) Energy Technologies Institute, 2018. Options, Choices, Actions. https://www.eti.co.uk/options-choices-actions-2018/

(53) GSEU Project, 2026. Map of CO2 storage potential areas (formation, units and traps) at the EU-scale. https://www.europe-geology.eu/data-tools/map-viewer/.

(54) Smith, A., Hampson, G. and Krevor, S., 2024. Global analysis of geological CO2 storage by pressure-limited injection sites. Int J Greenhouse Gas Control, 137, 104220. https://doi.org/10.1016/j.ijggc.2024.104220

(55) Evenick, J.C., 2021. Glimpses into Earth's history using a revised global sedimentary basin map. Earth-Sci. Rev. 215, 103564. https://doi.org/10.1016/j.earscirev.2021.103564

(56) IEA, 2015. Carbon Capture and Storage: The solution for deep emissions reductions (International Energy Agency Publications, Paris, 2015). 4

(57) Sharma, S., Van Gent, D., 2018. The Australian South West hub project: Developing confidence in migration assisted trapping in a saline aquifer - Understanding uncertainty boundaries through scenarios that stress the models. In 14th greenhouse gas control technologies conference. GHGT-14. October 21-26.

(58) Kivi, I.R., Makhnenko, R.Y., Oldenburg, C.M., Rutqvist, J. and Vilarrasa, V., 2022. Multi-layered systems for permanent geologic storage of CO2 at the gigatonne scale. Geophys. Res. Lett. 49(24), e2022GL100443. https://doi.org/10.1029/2022GL100443

(59) Pruess, K., 2008. Leakage of CO2 from geologic storage: Role of secondary accumulation at shallow depth. Int J Greenhouse Gas Control 2(1), 37-46. https://doi.org/10.1016/S1750-5836(07)00095-3

(60) Birkholzer, J.T., Zhou, Q., Tsang, C.F., 2009. Large-scale impact of CO2 storage in deep saline aquifers: A sensitivity study on pressure response in stratified systems. Int. J. Greenhouse Gas Control 3(2), 181-194. https://doi.org/10.1016/j.ijggc.2008.08.00

(61) Heddle, G., Herzog, H., Klett, M., 2003. The economics of CO2 storage. Massachusetts Institute of Technology, Laboratory for Energy and the Environment.

(62) Cihan, A., Birkholzer, J.T., Bianchi, M., 2015. Optimal well placement and brine extraction for pressure management during CO2 sequestration. Int. J. Greenhouse Gas Control 42, 175-187. https://doi.org/10.1016/j.ijggc.2015.07.025

(63) Bandilla, K.W., Celia, M.A., 2017. Active pressure management through brine production for basin-wide deployment of geologic carbon sequestration. Int. J. Greenhouse Gas Control 61, 155-167. https://doi.org/10.1016/j.ijggc.2017.03.030

(64) Birkholzer, J.T., Cihan, A., Zhou, Q., 2012. Impact-driven pressure management via targeted brine extraction—Conceptual studies of CO2 storage in saline formations. Int. J. Greenhouse Gas Control 7, 168-180. https://doi.org/10.1016/j.ijggc.2012.01.001

Supporting Information for

Coupled geophysical and technoeconomic growth constraints on geological carbon storage scaleup with an application to the UK

Iman R. Kivi[1,2*], Xiaowei Gao[2], Samuel Krevor[2]

[1]Global Change Research Group (GCRG), IMEDEA-CSIC-UIB, Esporles, Spain

[2]Department of Earth Science and Engineering, Imperial College London, London, UK

*Email of the corresponding author: iman.rahimzadeh@uib.es

S1. Dynamic storage resource assessment

In order to assess subsurface storage resources constrained by reservoir pressurisation and understand their control on achieving geologic CO_2 storage scaleup trajectories represented by growth models, we have adapted the analytical tool CO2BLOCK (Fig. S1). The tool was originally developed for simplified screening of subsurface CO_2 storage resources (De Simone et al., 2019; Kivi et al., 2025). It employs analytical solutions for two-phase flow of CO_2 and brine in saline aquifers under open and closed boundary flow conditions to calculate the spatial and temporal evolution of pore pressure around injection sites. By superimposing pressure fields of multiple injection sites, distributed in specific rectangular patterns and at varying distances across each of the storage regions, CO2BLOCK enables rapid evaluation and optimisation of basin-scale pressurisation under diverse injection scenarios. The analytical model for basin-scale pressure buildup estimates is explained in detail below.

Considering pressure buildup as the primary mechanism governing mechanical stability of subsurface structures, CO2BLOCK compares the estimated pressure evolution with rock failure criteria to identify the maximum sustainable injection rates. This modelling framework allows for an estimate of the storage capacity that can be safely achieved while maintaining the mechanical integrity of the storage complex. In particular, CO2BLOCK accounts for constraints imposed by caprock fracturing threshold and shear reactivation of pre-existing faults, which could compromise permanent containment of CO_2 deep underground or induce earthquakes.

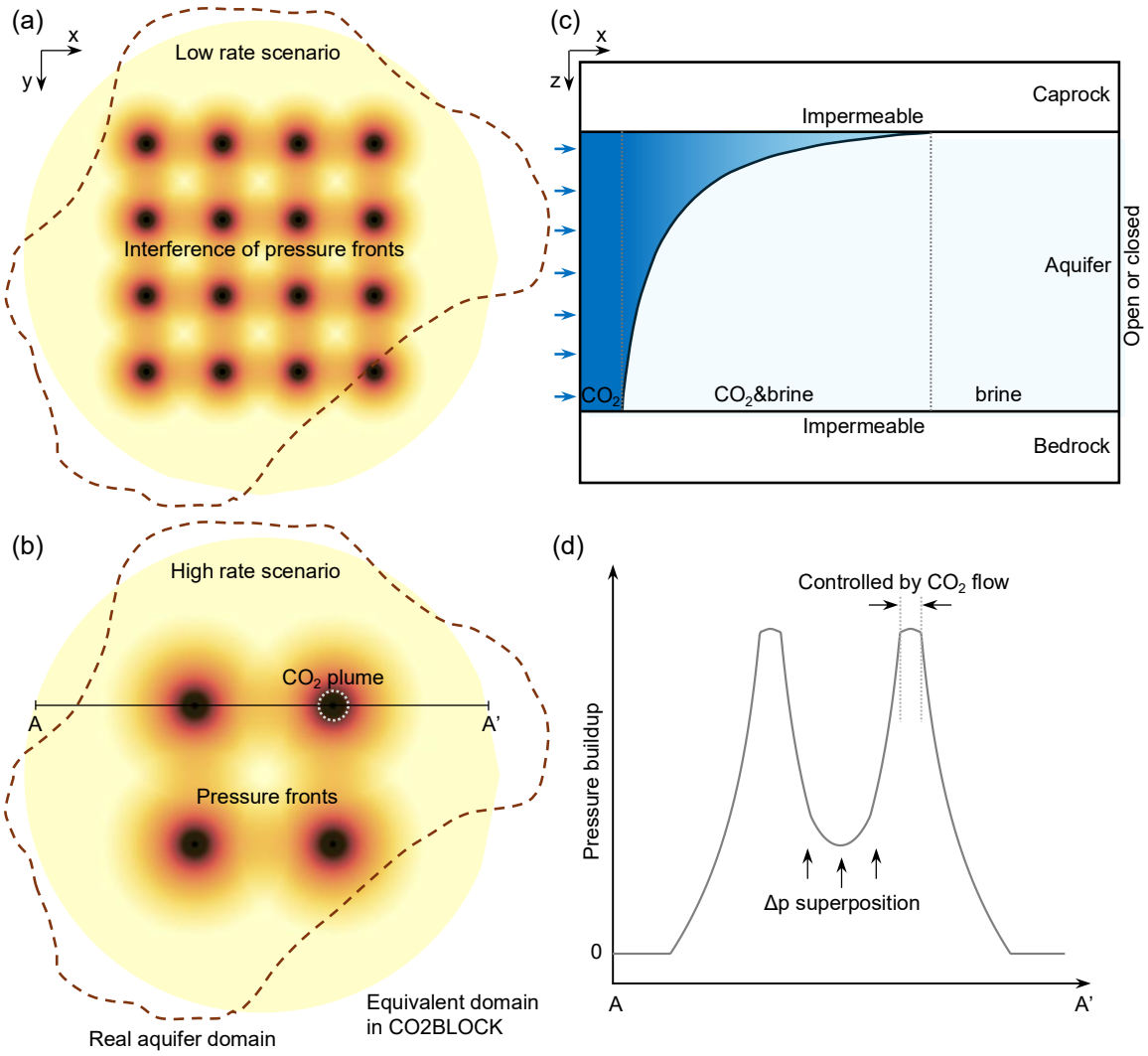

Fig. S1. Schematic illustration of the CO2BLOCK framework for estimating pressure-limited storage resources. (a,b) Examples of low- and high-rate injection scenarios illustrating the trade-off between the number of injection sites and their spacing. The dotted circle in panel (b) shows the extent of the CO_2 plume. CO2BLOCK evaluates sustainable storage resources across a range of site configurations. (c) Boundary flow conditions considered in the analytical pressure model for individual injection sites. (d) Analytical pressure profiles around injection sites, accounting for pressure interference using the superposition principle.

S1.1. Pressure buildup under open boundary flow conditions

The analytical model used in CO2BLOCK is adapted from Nordbotten et al. (2005) for CO_2 injection at a constant rate into an infinite, homogeneous, horizontal aquifer of constant thickness. The infinite-acting reservoir mimics open-flow boundary conditions. Injection is uniformly distributed across the entire height of the reservoir. Nordbotten et al. (2005) derived closed-form expressions for vertically averaged pressure build-up, assuming (1) instantaneous vertical equilibration of the phases under CO_2 gravity override, (2) a sharp CO_2-brine interface with each side of the interface fully saturated with the respective fluid, and (3) constant fluid densities and viscosities for each phase. These expressions specify three reservoir regions with distinct pressure trends: (1) adjacent to the wellbore, fully saturated by CO_2, (2) a transition region where the two fluids coexist, and (3) the far-field, fully saturated by brine (Nordbotten et al., 2005; Vilarrasa et al., 2010). This solution can be further simplified by replacing the transition zone with a fictitious equivalent vertical interface, which yields (De Simone et al., 2019)

$$\Delta p^{\infty}(r,t) = \frac{Q\mu_b}{2\pi kH\rho_c} \times \Delta p^{*}(t,r), \qquad \text{Eq. (S1)}$$

where

$$\Delta p^{*}(t,r) = \begin{cases} \frac{\mu_c}{\mu_b}\ln\left(\frac{\psi}{r}\right) + \ln\left(\frac{R}{\psi}\right) & , r \le \psi \\ \ln\left(\frac{R}{r}\right) & , \psi < r \le R \\ 0 & , R < r. \end{cases} \qquad \text{Eq. (S2)}$$

In these expressions, $\Delta p^{\infty}(r,t)$ is the pressure change at time t and distance r from the wellbore under open flow boundary conditions, Q is the mass flow rate, k is the absolute reservoir permeability, H is the reservoir thickness, ρ_c is the average CO_2 density across the plume, μ_b and μ_c are the average brine and CO_2 dynamic viscosities, respectively, $R =$

$\sqrt{2.25kt/(\mu_b(c_r + \phi c_b))}$ is the radius of influence over which pressure diffusion propagates at time t, ϕ is the rock porosity, c_r and c_b are rock and brine compressibilities, respectively, and ψ is the radius of the fictitious equivalent vertical interface and is given by

$$\psi = \xi e^{\theta}, \quad \text{Eq. (S3)}$$

where $\xi = \sqrt{Qt/(\pi\phi H\rho_c)}$ is the extent of advective propagation of the cylindrical CO_2 front and $\theta = (\mu_c + \mu_b)/(\mu_c - \mu_b)\ln(\sqrt{\mu_c/\mu_b}) - 1$ represents a function of fluid mobilities. The density and viscosity of the fluids are estimated at the mean reservoir pressure, temperature, and salinity.

The performance of this simplified solution has been verified against numerical simulations (De Simone et al., 2019). Pore pressure varies logarithmically with distance from the injection wellbore. Thus, plotting pore pressure versus the logarithm of distance results in a bilinear curve with a sharp change in slope due to the fluid viscosity change at $r = \psi$. The original Nordbotten et al. (2005) solution returns the same estimates of pore pressure in the near-wellbore and far-field regions, but slightly different estimates in the transition zone as fluid viscosity is represented by a linear weighted average between those of brine and CO_2. We here use the compacted version of the solution (De Simone et al., 2019) as it simplifies calculations in a straightforward manner.

S1.2. Multi-site injection configurations

For multi-site injection, the pressure response at any location is obtained by applying the principle of linear superposition to the individual well solutions. To this end, Eqs. 1-3 are evaluated independently for each injection site using the corresponding distance to the observation point, and the resulting pressure contributions are summed to obtain the total

pressure buildup. For two-phase flow, which is inherently a non-linear phenomenon, the superposition approaximation results in an error whose magnitude grows with the number of injection sites (De Simone et al., 2019). The error arises because the pressure solution associated with each injection site is evaluated independently, neglecting the increased fluid mobility produced by CO_2 plumes around neighbouring injection sites. Consequently, pressure propagation in the far-field is no longer controlled solely by brine viscosity, as assumed in Eq. S2. Instead, the presence of intervening CO_2 plumes locally increase fluid mobility, reducing hydraulic resistance and attenuating pressure buildup. Neglecting this effect causes the superposition approach to systematically overestimate pressure buildup, resulting in conservative estimates of storage complex integrity.

S1.3. Extension to closed boundary flow conditions

For closed boundary flow conditions, pressure diffusion is confined within a finite aquifer volume and the injected CO_2 is accommodated by compression of the resident brine and the rock framework. In the initial version of CO2BLOCK, closed-boundary effects were approximated by adding a finite-domain correction factor to the dimensionless pressure response of the single-site Nordbotten solution (Eq. 2). The correction factor f_{cb} evolves with time as (De Simone and Krevor, 2021)

$$f_{\mathrm{cb}}(t) = \frac{2R^2}{2.25R_c^2} - \frac{3}{4}, \qquad \text{Eq. (S4)}$$

where R_c is the radius of the equivalent circular closed reservoir and time enters the expression through the radius of influence R. Inspired by pseudo-steady-state, single-phase radial flow in a closed reservoir (Zimmerman, 2018), this correction can provide a reasonable approximation for a single injection site located at the centre of a circular closed reservoir. However, its direct

application to multi-site injection configurations incurs error in pressure estimates. This is because each injection site is treated as if it were centred in its own equivalent closed reservoir, whereas in reality all sites pressurise a single bounded storage volume. In other words, direct superposition of single-site closed-boundary corrections virtually expands the pressurised reservoir volume, rather than treating the aquifer as one shared closed system. As a result, the superposed pressure field is not effectively constrained by the reservoir-wide material balance, resulting in an underestimation of pressure buildup. This underestimation translates into an overestimation of reservoir injectivity and, thus, larger estimates of pressure-limited CO_2 storage resources.

To resolve this issue, in CO2BLOCK-GROWTH, we reformulate the closed-boundary pressure response by adapting the decomposition concept proposed for decline curve analysis in multi-well hydrocarbon production fields (Marhaendrajana and Blasingame, 2001). This concept relies on the notion that a multi-well system can be represented by the aggregated response of a single well in a closed system only when the total material balance of the reservoir is enforced. Accordingly, we decompose the pressure field into a spatially averaged bulk-pressure component, $\Delta\bar{p}(t)$, and a zero-mean dynamic component, $\Delta p'(r,t)$, as

$$\Delta p(r,t) = \Delta\bar{p}(t) + \Delta p'(r,t). \quad \text{Eq. (S5)}$$

By definition,

$$\Delta\bar{p}(t) = \frac{1}{A}\int_{\Omega} \Delta p(r,t)\, dA, \quad \text{Eq. (S6)}$$

and therefore

$$\frac{1}{A}\int_{\Omega} \Delta p'(r,t)\, dA = 0. \quad \text{Eq. (S7)}$$

The average pressure term represents the uniform reservoir-scale pressure increase consistent with the global material balance equation. For a total mass injection rate $Q_{\mathrm{tot}} = NQ$, where N is the number of injection sites, this term is calculated as

$$\Delta\bar{p}(t) = \frac{Q_{\mathrm{tot}}t}{\rho_c AH(c_r+\phi c_b)}, \qquad \text{Eq. (S8)}$$

where A is the reservoir area. This bulk-pressure term is applied only once for the entire reservoir as all injection sites share the same closed compressible volume.

On the other hand, the dynamic pressure component is approximated using the open-boundary Nordbotten solution (Eqs. S1-S3) after removal of its spatial mean over the actual closed reservoir domain Ω, which writes as

$$\langle \Delta p_i^{\infty} \rangle_{\Omega} = \frac{1}{A}\int_{\Omega_i^{eff}} \Delta\, p_i^{\infty}(r,t)\, dA, \qquad \text{Eq. (S9)}$$

where Ω_i^{eff} denotes the pressure-influence region of site i that lies inside the actual reservoir domain (Fig. S2). It is then straightforward to write the zero-mean local contribution from site i to the pressure change as

$$\Delta p_i'(r,t) = \Delta p_i^{\infty}(r,t) - \langle \Delta p_i^{\infty} \rangle_{\Omega}. \qquad \text{Eq. (S10)}$$

This pressure component accounts for the dynamics of pressure evolution around each individual injection site. The total pressure buildup under closed boundary flow conditions is finally calculated as

$$\Delta p(r,t) = \frac{Q_{\mathrm{tot}}t}{\rho_c AH(c_r+\phi c_b)} + \sum_{i=1}^{N} \Delta p_i'(r,t). \qquad \text{Eq. (S11)}$$

The proposed formulation provides a computationally efficient approximation for closed-boundary flow conditions. It enforces the correct reservoir-scale material balance while retaining local pressure interference through superposition of the zero-mean dynamic pressure

contributions. Further improvements could be achieved by deriving exact closed-domain Green's functions for multiphase flow.

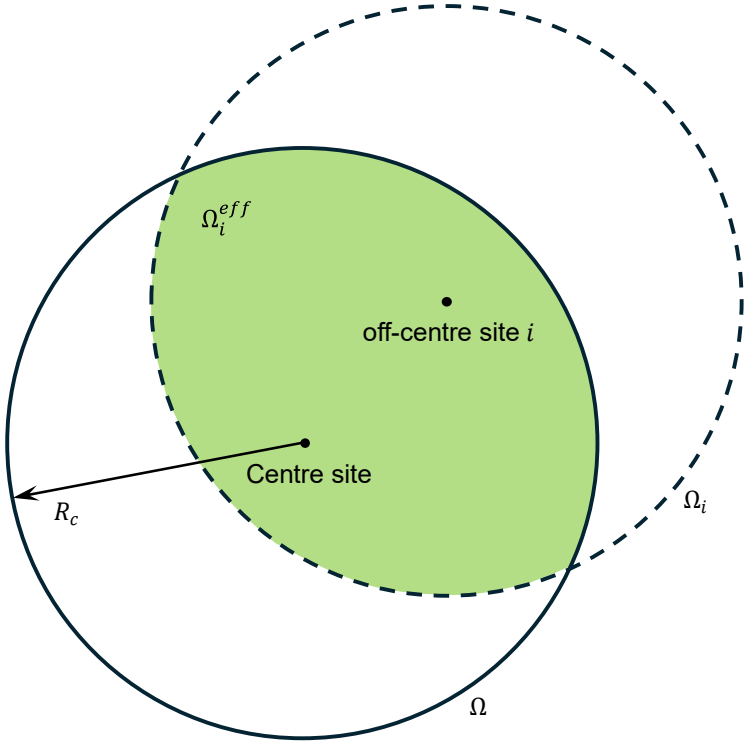

Fig. S2. Schematic illustration of the effective pressurised domain Ω_i^{eff} associated with an off-centre injection site under closed boundary conditions. The effective domain is the area over which the contribution of site i to pressure buildup is integrated to compute the spatially averaged pressure contribution that is subtracted from the dynamic pressure term. This area corresponds to the intersection between the pressure domain of injection site i (dashed circle) and the actual closed reservoir domain (solid circle).

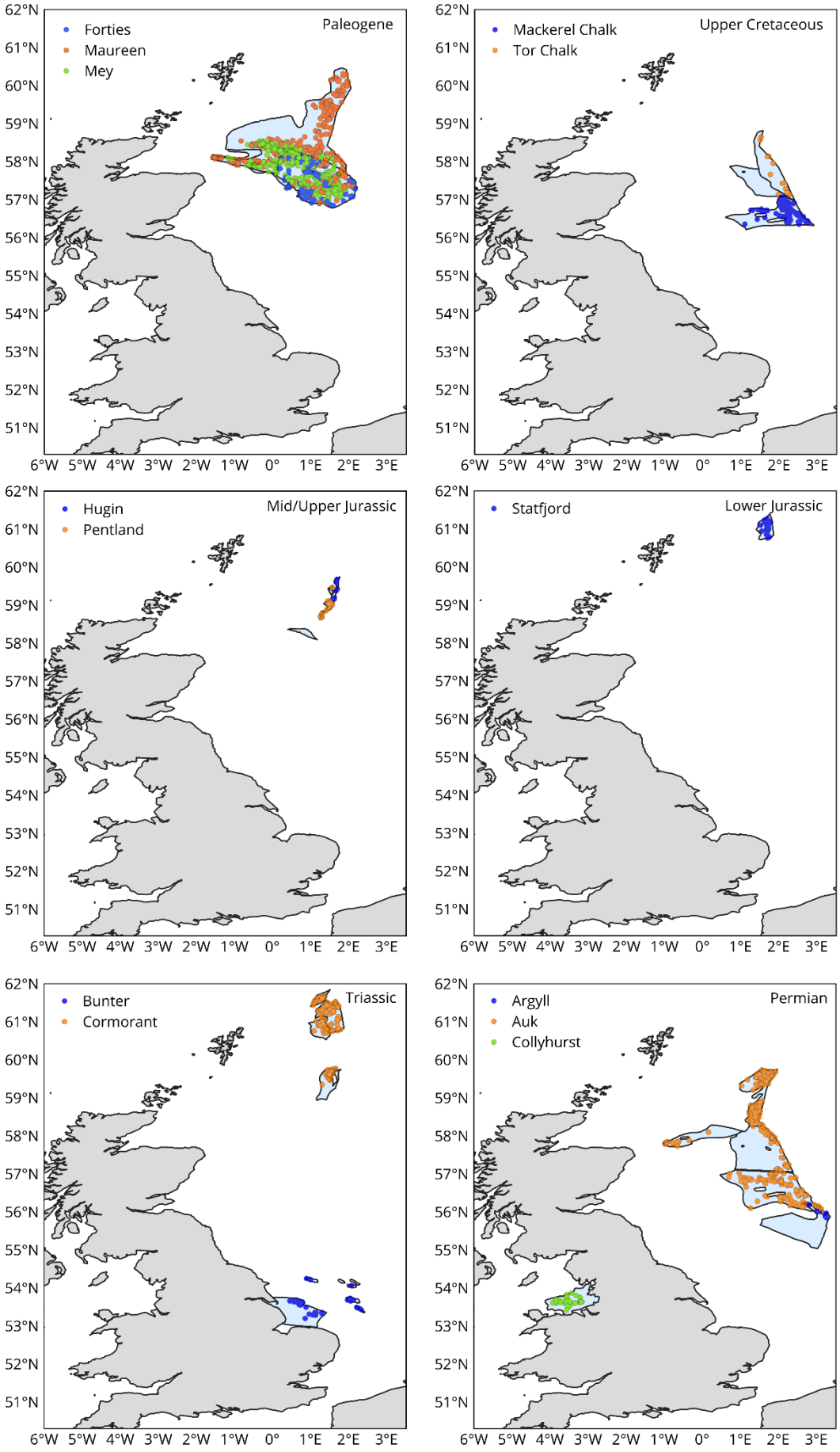
Paleogene
Forties
Maureen
Mey
Upper Cretaceous
Mackerel Chalk
Tor Chalk
Mid/Upper Jurassic
Hugin
Pentland
Lower Jurassic
Statfjord
Triassic
Bunter
Cormorant
Permian
Argyll
Auk
Collyhurst
62°N
61°N
60°N
59°N
58°N
57°N
56°N
55°N
54°N
53°N
52°N
51°N
6°W 5°W 4°W 3°W 2°W 1°W 0° 1°E 2°E 3°E

Fig. S3. Spatial distribution of wellbores in UK offshore CO_2 storage aquifers by geological age.

S2. Parameterisation of the geophysical model for the UK storage units

Saline aquifers are usually not extensively characterised, and uncertainties in parameters can result in order of magnitude variations in dynamic estiamtes of the storage resource base (De Simone and Krevor, 2021). We parameterise our calculations based primarily on data reported in the CO_2Stored database (Bentham et al., 2014; Energy Technologies Institute, 2018). The database provides likely values for geometrical parameters such as formation areal extent and thickness, as well as hydraulic characteristics such as rock porosity, permeability, compressibility and boundary flow conditions. Yet, these parameters may bear uncertainty to varying extents in estimates of storage formation pressure response to CO_2 injection. In particular, rock permeability is known to vary across spatial scales. While addressing scale-dependent permeability of the rock mass entails site-specific studies, we explore sensitivity of injection-induced pressure buildup to uncertainty in the permeability field by considering three alternative models where the permeability, k, is conservatively reduced by factors of 2, 5 and 10 –referred to as $k/2$, $k/5$ and $k/10$ models.

Hydraulic and geometrical parameters vary substantially across the selected UK storage units (Fig. S4). Average reservoir porosity spans a range of roughly 0.15, and permeability ranges over several hundred millidarcies. While these hydraulic attributes exhibit largely random spatial distributions, the geometrical characteristics of the storage units display meaningful regional trends across the four UK offshore sectors. In particular, the central and northern North Sea show markedly greater variability. These regions host several laterally extensive and thick storage units, with some exceeding 1 km in thickness in the Northern basin.

Furthermore, they are systematically deeper, with most units located below 2 km and some extending to ~3.5 km. These trends indicate that central and northern basins may offer considerable storage potential, although their development is likely to be more technically and economically demanding.

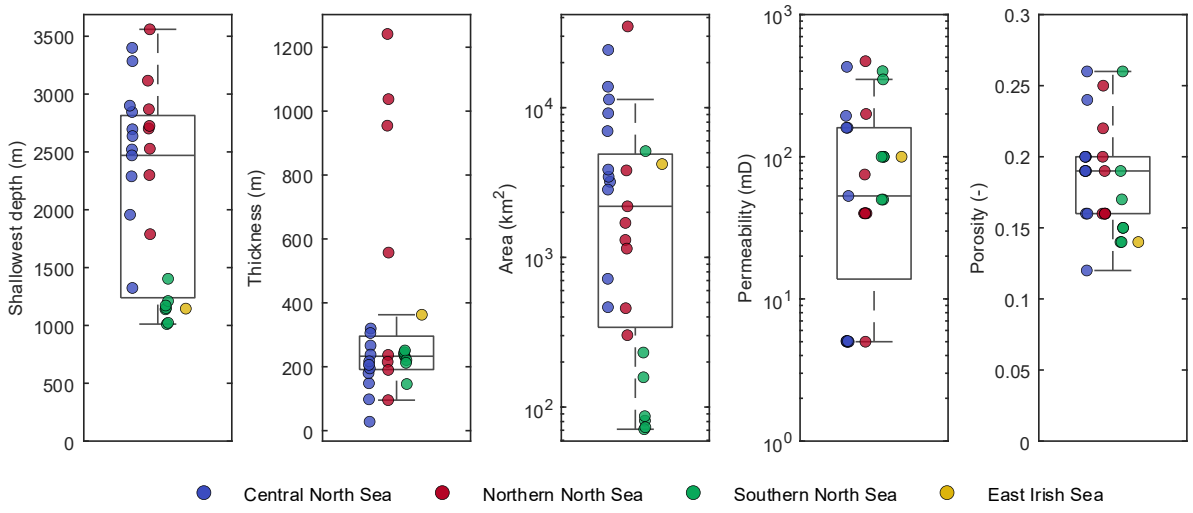

Fig. S4. Boxplot for a number of key parameters controlling reservoir pressure response to CO_2 injection, including shallowest reservoir depth, its thickness, areal extent, intrinsic permeability and porosity. From bottom to top, the box indicates the first quartile, median and third quartile of the data. Whiskers represent the minimum and maximum values, excluding outliers. Outliers are defined as data residing outside the range defined by 1.5 times the interquartile range beyond the first and third quartiles.

In contrast to hydraulic properties, information about geomechanical parameters is commonly lacking as they are more difficult to estimate. These parameters determine the susceptibility of the storage unit to mechanical failure in response to injection pressure. We conservatively assume that the formation is cohesionless and is crossed by optimally oriented faults to slip at the location of the largest pressure buildup across each study area. We adopt a representative fault friction angle of 30º (Jaeger et al., 2009). Eventually, the largest uncertainty is introduced by the state of stress, particularly, the ratio of the minimum to maximum effective

principal stress $S = \sigma'_3/\sigma'_1$, hereinafter referred to as the stress ratio, which imposes first-order control on reservoir integrity calculations. While initial reservoir pressure and overburden stress are reported for candidate storage units in the CO_2Stored database, we use public stress records at the regional scale to constrain the stress ratio for the regions of interest.

The North Sea is a relatively stable intraplate sedimentary basin, generally regarded as tectonically relaxed compared with other continental margins (Edwards et al., 1998). As a result, its present-day stress field is dominated by a tensile (normal) regime in the southern and central sectors, where the vertical stress, σ_v, slightly exceeds the maximum and minimum horizontal components, σ_H and σ_h, respectively, and horizontal stress anisotropy remains low, i.e., $\sigma_v > \sigma_H \approx \sigma_h$ (Fig. S5; Hillis and Nelson, 2005; Williams et al., 2015; Fellgett et al., 2018). Direct measurements of the minimum horizontal stress, σ_h, from (extended) leak-off tests indicate relatively high stress ratios, with a representative value of 0.78 in the southern North Sea and ranging between 0.5 and 0.9 under variable pore pressure, with an average of 0.71 in the central basin (Edwards et al., 1998). Toward the northern North Sea, the stress regime transitions to a more compressional state ($\sigma_H > \sigma_v \approx \sigma_h$), indicative of strike-slip to reverse faulting conditions (Fig. S5; Wiprut and Zoback, 2000; Hillis and Nelson, 2005). This transition is primarily attributed to deglaciation stress effects (Hillis and Nelson, 2005) and far-field compression associated with the Atlantic ridge push (Fejerskov and Lindholm, 2000). Estimates of the maximum horizontal stress, σ_H, remain sparse, as its determination is less straightforward than for other stress components. Extensive analyses of data from boreholes in the Visund field (Norwegian sector) suggest significant horizontal stress anisotropy with a factor of 1.25 (Wiprut and Zoback, 2000). Given that tectonic activity is less pronounced in the UK sector, this stress field likely represents a lower-bound estimate of the stress ratio in the northern North Sea and is adopted here for conservative estimates of storage resources. A similar transition from strike-slip to reverse stress regimes seems to prevail in the East Irish

Sea Basin (Williams et al., 2018). In the absence of sufficient data to contrain σ_H, we take the same stress field as in the northern North Sea for this region. Accordingly, we calculate stress ratios ranging from $S = 0.37$ to $S = 0.65$ with an average of $S = 0.53$ in these regions.

The vertical stress generally follows an average gradient of approximately 21 MPa/km. Reservoir pressures in the southern North Sea and East Irish Sea units are close to hydrostatic conditions, whereas pressure anomalies are observed in several units within the northern and central basins (Fig. S5). It is broadly demonstrated that horizontal stresses tend to increase with pressure abnormality (Zoback, 2010), reflecting the coupled response of the stress field to pore pressure variations. Thus, our estimates of the stress ratio, derived from minimum horizontal stress data in normally pressured settings, likely underestimate the true stress ratios and in this regard are conservative in the resource assessment. Units exhibiting elevated pressures are represented by Mohr circles located closer to the frictional failure envelope, indicating reduced capacity for CO_2 injection while preserving the mechanical stability of the storage complex (see inset in Fig. S5).

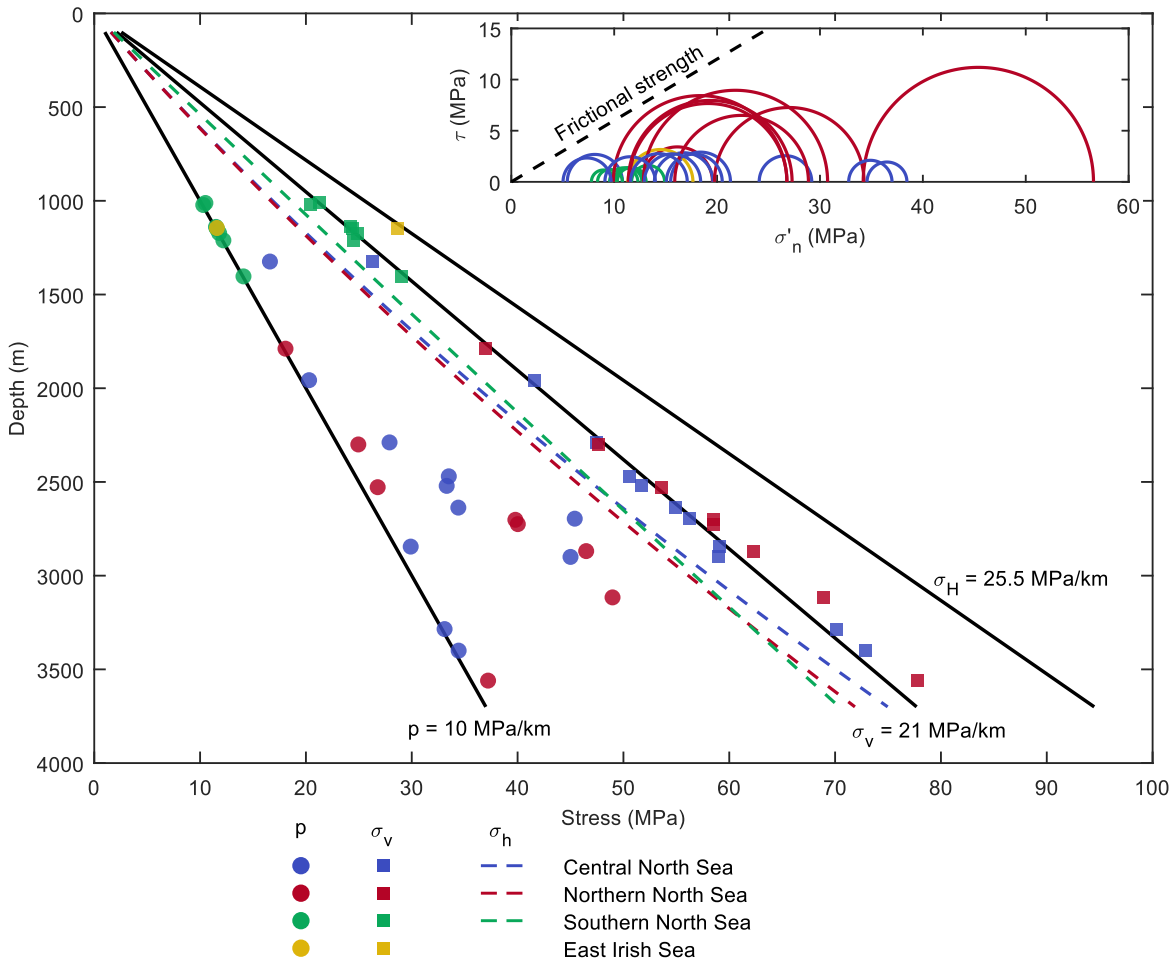

Fig. S5. In situ stress and pore pressure conditions in four UK offshore regions for CO_2 storage: central North Sea, northern North Sea, southern North Sea, and East Irish Sea. Average overburden stress (σ_v), hydrostatic pressure (p), measured minimum horizontal stress across the North Sea (σ_h) and maximum horizontal stress (σ_H) profiles are plotted as a function of depth (continuous lines), together with measured pore pressure and overburden stress at the shallowest depths of candidate reservoir units across the four regions (discrete symbols). The inset illustrates corresponding Mohr circles for 27 storage units, colored by region, and the frictional strength envelope ($\mu = 0.6$).

S3. Injectivity analysis of UK offshore storage units

Simulation results show that reservoir injectivity, defined as the achievable injection rate per unit increase in reservoir pressure, is governed jointly by reservoir properties, boundary flow conditions, and the spatial configuration of injection sites. In scenarios with few injection sites, where lateral pressure interference between individual sites is minimal, per-site injectivity is primarily controlled by intrinsic reservoir characteristics. In a storage unit like Auk 029 15 with relatively low intrinsic rock permeability (~5 mD) and closed flow boundaries, despite its large thickness (180 m) and large areal extent (~11,000 km^2), as well as favourable stress conditions (high stress ratio of 0.71), injection rate per site is limited to nearly 1.2 Mt yr^{-1} to maintain mechanical integrity (Fig. S6a). In contrast, Mey 5 exhibits high permeability (>400 mD), substantial thickness (~220 m), and open boundary conditions over a very large area (~24,000 km^2), which enables per-site injection rates as large as the model-imposed upper limit of 20 Mt yr^{-1} for up to ~12 injection sites without exceeding the critical pressure (Fig. S6b).

Feasible injection scenarios are principally constrained by the reservoir surface area, which imposes an upper bound on the allowable combinations of site number and spacing (blue lines in Fig. S6). The maximum per-site injectivity generally decreases with increasing number of injection sites across possible scenarios because of growing pressure interference resulting from shortening inter-site distances. Nevertheless, maximum storage capacity does not necessarily follow the same trend. For both example sites, the maximum cumulative storage capacity is achieved by deploying a large number of injection sites operating near the minimum per-site injection rate of 1 Mt yr^{-1} (Fig. S6). This trend shows that maximizing the total accessible reservoir area is generally more beneficial than maximizing injectivity at individual sites. Such dominance of total injection area over local injectivity loss is similarly observed in several other storage units with either open or closed boundaries (Table S1). However, smaller, closed-boundary reservoirs such as Hugin 009 18 and the Pentland units show markedly

different behaviour. In these cases, the sharp reduction in per-site injectivity associated with additional sites outweighs the benefit of increasing the number of injectors. As a result, the optimal strategy in these cases consists of deploying only a few high-rate injection sites (Table S1).

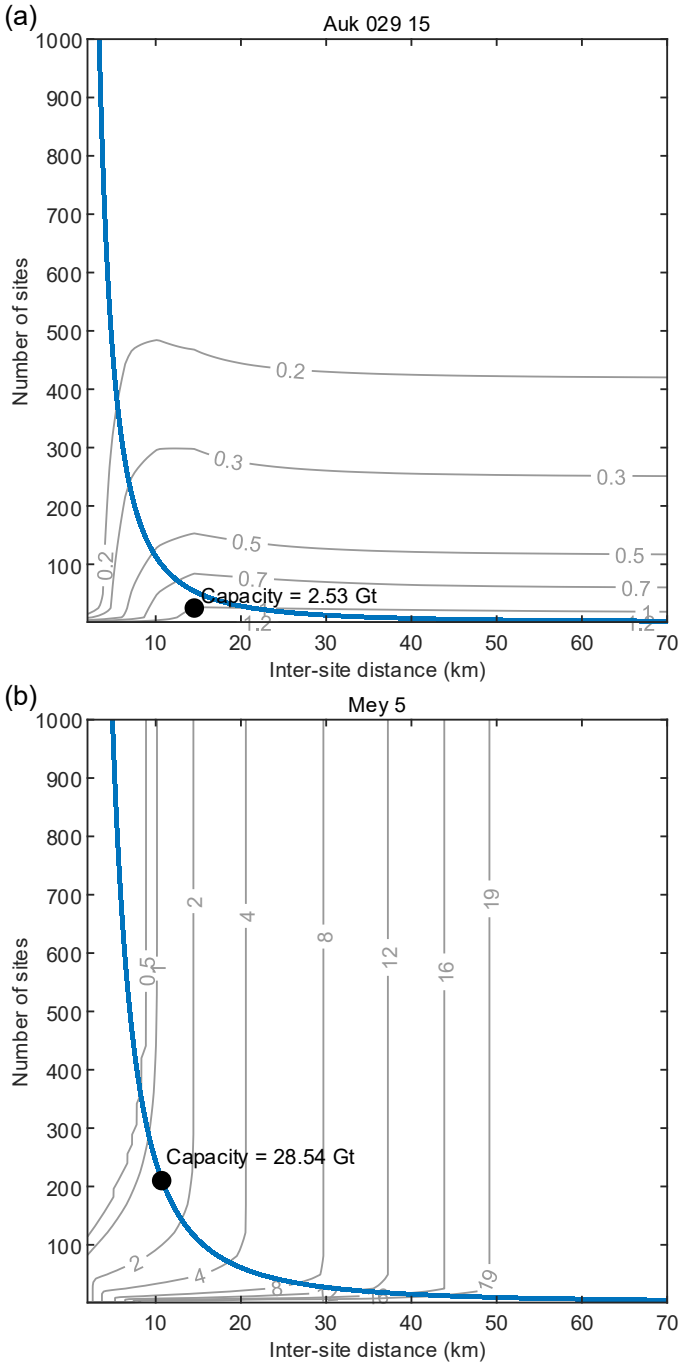

Fig. S6. Reservoir injectivity calculations for 100 years of continuous injection into (a) Auk 029 15 and (b) Mey 5 as representative examples of storage units with closed and open

boundary flow conditions, respectively, under different scenarios of injection patterns defined by the number and distance between the sites. Contours show injection rate per site (Mt yr^{-1}) and the blue line draws an upper bound limit to possible site numbers given the reservoir areal extent, i.e., possible scenarios reside to the left and below the blue line. The maximum storage capacity that can be achieved is shown by a filled circle.

Table S1. Maximum storage capacity, injection rate per site, and corresponding number and distance of sites required to achieve these rates for the selected UK storage locations. Calculations assume 100 years of continuous injection and a prescribed minimum intersite spacing of 2 km. Note that storage capacities denoted by "-" imply units that cannot maintain injection rates above the minimum threshold of 1 Mt yr^{-1} for 100 years even with one injection site.

Unit name	Capacity (Gt)	Rate per site (Mt yr^{-1})	Site number	Distance (km)	Boundary
Argyll 038 14	0.93	1.04	9	27.8	Closed
Auk 009 28	0.42	1.05	4	15	Closed
Auk 020 05	-	0.86	1	2	Closed
Auk 022 13	-	0.33	1	2	Closed
Auk 029 15	2.53	1.01	25	14.5	Closed
Bunter Closure 28	0.14	1.37	1	2	Closed
Bunter Closure 3	-	0.50	1	2	Closed
Bunter Closure 35	0.11	1.13	1	2	Closed
Bunter Closure 36	-	0.64	1	2	Closed
Bunter Closure 37	-	0.87	1	2	Closed
Bunter Closure 39	-	0.79	1	2	Closed
Bunter SS Fm Zone 1	4.99	1.19	42	11	Open
Collyhurst SS Fm 1	4.87	1.16	42	9.9	Closed
Cormorant 003 02	0.54	1.35	4	18	Closed
Cormorant 009 18	7.07	1.1	64	5.1	Closed
Cormorant 211 12	0.55	1.38	4	10.6	Closed
Cormorant 211 23	1.28	1.06	12	13.4	Closed
Forties 5	1.90	1.19	16	29.3	Open
Hugin 009 18	0.55	1.37	4	8.7	Closed
Mackerel Chalk 022 15	2.17	1.08	20	11.9	Open
Maureen 2	14.03	1.28	110	17.7	Open
Mey 5	28.54	1.36	210	10.7	Open
Pentland 009 28	2.46	2.74	9	8.9	Closed
Pentland 016 21b	1.02	2.54	4	10.7	Closed
Statfjord 211 23	0.22	1.1	2	23.8	Closed
Tor Chalk 022 018	4.56	1.09	42	9	Open
Tor Chalk 022 09	-	0.89	1	2	Open

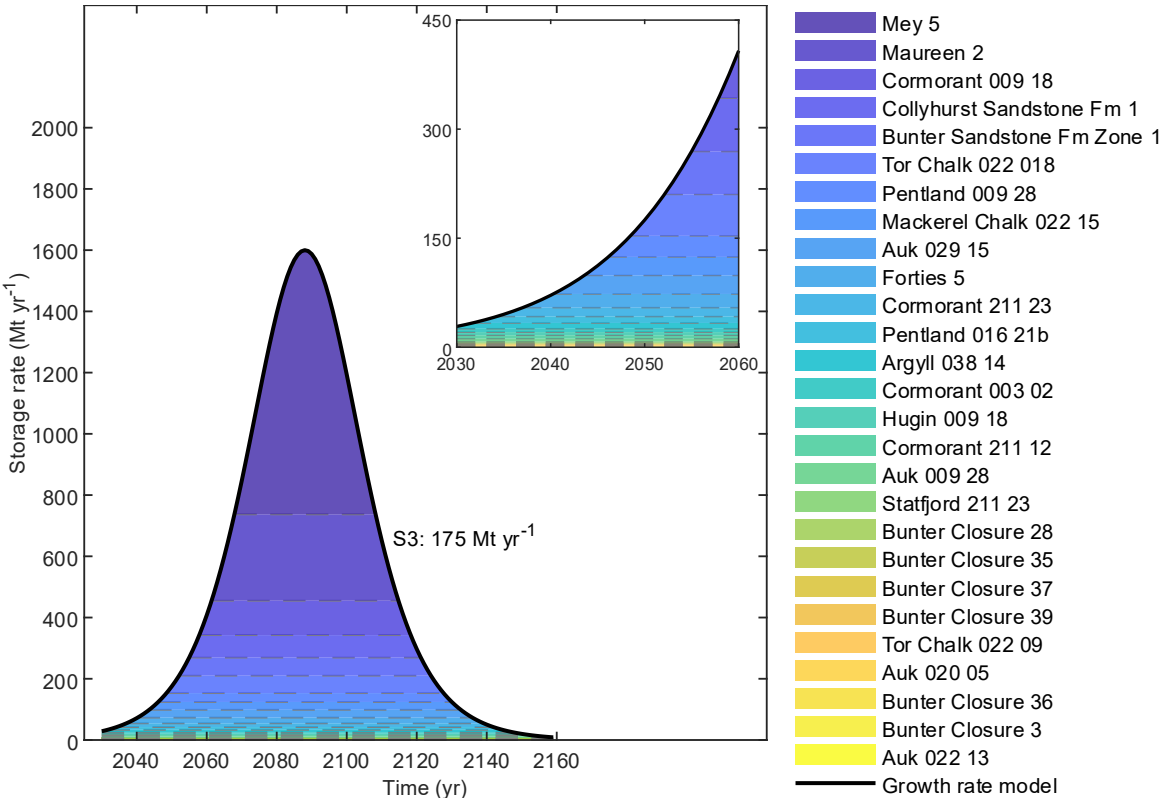

Fig. S7. Resource allocation under the growth rate model targeting a 2050 storage rate of 175 Mt yr^{-1} and a cumulative storage amount of 69 Gt, for the scenario prioritising units with smallest storage capacities. Inset shows zoomed view of the plot during the early stages of injection. Labels on the plot show the number of sites required to address the growth trajectory.

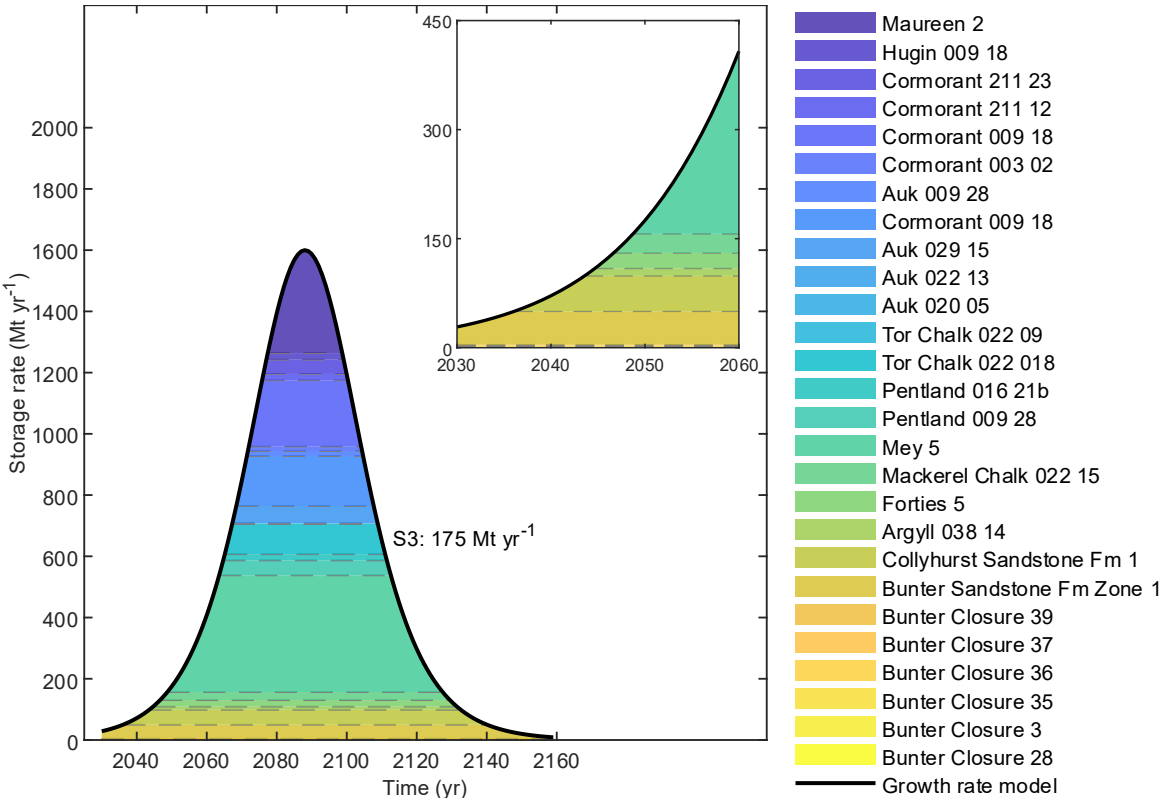

Fig. S8. Resource allocation under the growth rate model targeting a 2050 storage rate of 175 Mt yr^{-1} and a cumulative storage amount of 69 Gt, for the scenario consistent with planned projects, prioritising units in the southern North Sea, East Irish Sea, central North Sea, and northern North Sea, respectively. Inset shows zoomed view of the plot during the early stages of injection.

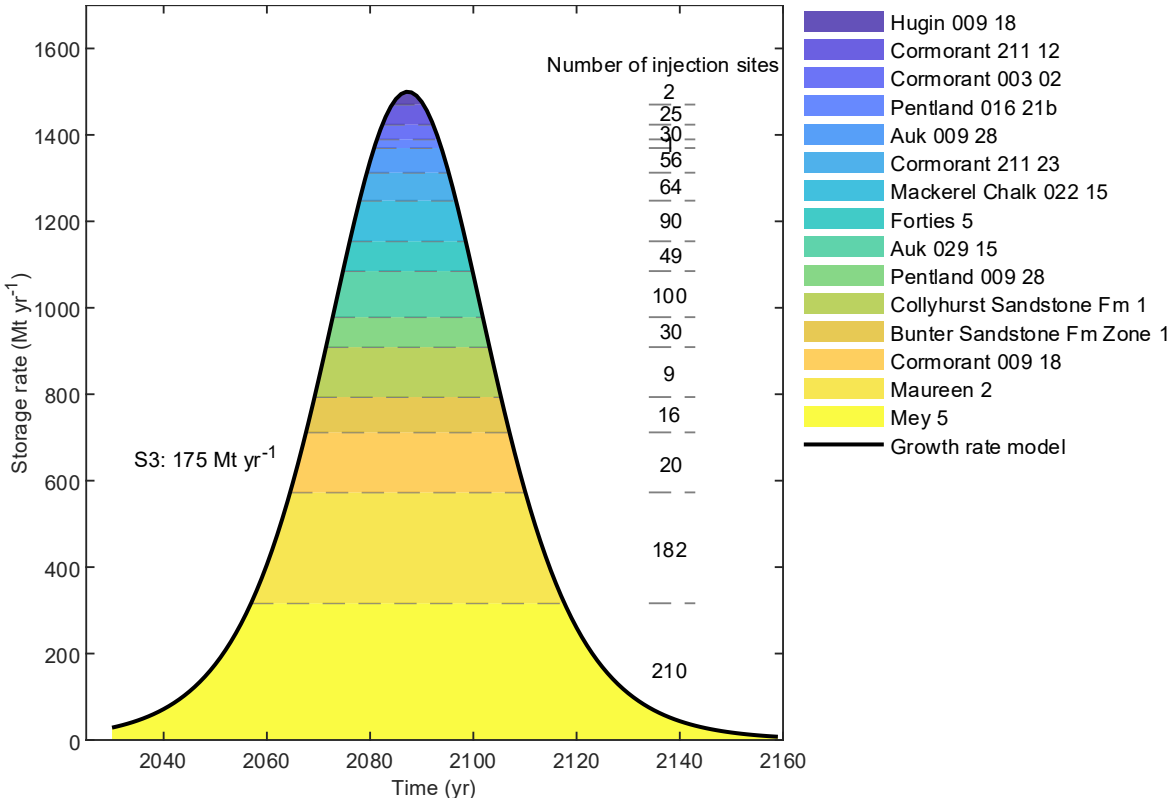

Fig. S9. Resource allocation for the growth rate model with a 2050 storage rate target of 175 Mt yr^{-1} and a cumulative storage amount of 64 Gt, when the maximum possible number of storage sites is constrained to historically drilled hydrocarbon wells in each region.

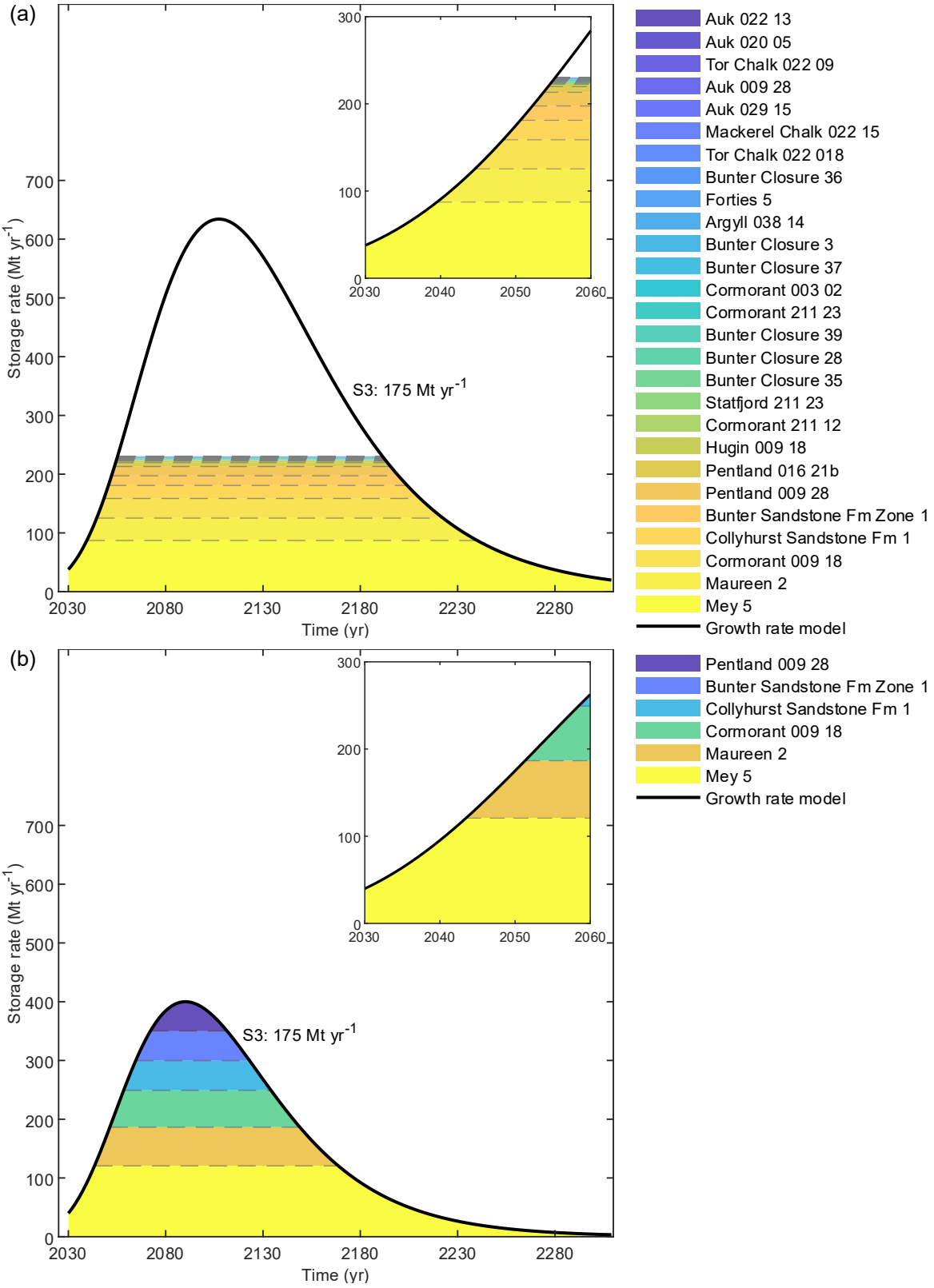

Fig. S10. Resource allocation for the Gompertz model targeting a CO_2 storage rate of 175 Mt yr^{-1} by 2050 and a (a) cumulative storage mass of 78 Gt, and (b) cumulative storage mass of 41 Gt, both considering reduced reservoir permeability by an order of magnitude ($k/10$

scenario). Comparison between the two panels shows how uncertainties in the permeability could affect addressing long-term scaleup trajectories. Insets show zoomed views of the plots during the early stages of injection.

References for supporting information

Bentham, M., Mallows, T., Lowndes, J., Green, A., 2014. CO_2 STORage evaluation database (CO_2 Stored). The UK's online storage atlas. Energy Procedia, 63, 5103-5113. https://doi.org/10.1016/j.egypro.2014.11.540

De Simone, S., Jackson, S.J., Krevor, S., 2019. The error in using superposition to estimate pressure during multi-site subsurface CO_2 storage. Geophys. Res. Lett. 46 (12), 6525–6533. https://doi.org/10.1029/2019GL082738

De Simone, S., Krevor, S., 2021. A tool for first order estimates and optimisation of dynamic storage resource capacity in saline aquifers. Int. J. Greenhouse Gas Control 106, 103258. https://doi.org/10.1016/j.ijggc.2021.103258

Edwards, S.T., Meredith, P.G., Murrell, S.A.F., 1998. An investigation of leak-off test data for estimating in-situ stress magnitudes: application to a basinwide study in the North Sea. In SPE/ISRM Rock Mechanics in Petroleum Engineering 1998 July 8 (pp. SPE-47272). SPE.

Energy Technologies Institute, 2018. Options, Choices, Actions. https://www.eti.co.uk/options-choices-actions-2018/

Fejerskov, M., Lindholm, C., 2000. Crustal stress in and around Norway: an evaluation of stress-generating mechanisms. In Dynamics of the Norwegian Margin. Nøttvedt, A. https://doi.org/10.1144/GSL.SP.2000.167.01.19

Fellgett, M.W., Kingdon, A., Williams, J.D. and Gent, C.M., 2018. Stress magnitudes across UK regions: New analysis and legacy data across potentially prospective unconventional resource areas. Mar. Pet. Geol. 97, 24-31. https://doi.org/10.1016/j.marpetgeo.2018.06.016

Hillis, R.R. and Nelson, E.J., 2005. In situ stresses in the North Sea and their applications: Petroleum geomechanics from exploration to development. In Petroleum Geology: North-West Europe and Global Perspectives—Proceedings of the 6th Petroleum Geology Conference, A. G. Doré, B. A. Vining. https://doi.org/10.1144/0060551

Jaeger, J.C., Cook, N.G., Zimmerman, R., 2009. Fundamentals of rock mechanics. John Wiley & Sons.

Kivi, I.R., De Simone, S., Krevor, S., 2025. A simplified physics model for estimating subsurface CO_2 storage resources constrained by fault slip potential. J. Rock Mech. Geotech. Eng. 18(4), 2546-2560. https://doi.org/10.1016/j.jrmge.2025.06.031

Marhaendrajana, T., Blasingame, T.A., 2001. Decline curve analysis using type curves—evaluation of well performance behavior in a multiwell reservoir system. In SPE Annual Technical Conference and Exhibition? (pp. SPE-71517). SPE.

Nordbotten, J.M., Celia, M.A., Bachu, S., 2005. Injection and storage of CO_2 in deep saline aquifers: analytical solution for CO_2 plume evolution during injection. Transp. Porous Med. 58 (3), 339–360. https://doi.org/10.1007/s11242-004-0670-9

Vilarrasa, V., Bolster, D., Dentz, M., Olivella, S., Carrera, J., 2010. Effects of CO_2 compressibility on CO_2 storage in deep saline aquifers. Transp. Porous Med. 85 (2), 619–639. https://doi.org/10.1007/s11242-010-9582-z

Williams, J.D.O., Fellgett, M.W., Kingdon, A., Williamson, J.P., 2015. In-situ stress orientations in the UK Southern North Sea: Regional trends, deviations and detachment of the

post-Zechstein stress field. Mar. Pet. Geol. 67, 769-784. https://doi.org/10.1016/j.marpetgeo.2015.06.00

Williams, J.D.O., Gent, C.M.A., Fellgett, M.W. and Gamboa, D., 2018. Impact of in situ stress and fault reactivation on seal integrity in the East Irish Sea Basin, UK. Mar. Pet. Geol. 92, 685-696. https://doi.org/10.1016/j.marpetgeo.2017.11.030

Wiprut, D., Zoback, M.D., 2000. Fault reactivation and fluid flow along a previously dormant normal fault in the northern North Sea. Geology 28(7), 595-598. https://doi.org/10.1130/0091-7613(2000)28<595:FRAFFA>2.0.CO;2

Zimmerman, R. (2018). The Imperial College lectures in petroleum engineering. volume 5: Fluid flow in porous media. World Scientific Publishing Europe. https://doi.org/10.1142/q0146

Zoback, M.D., 2010. Reservoir geomechanics. Cambridge university press.